
Article:
Borhani, T.N., Oko, E. orcid.org/0000-0001-9221-680X and Wang, M. orcid.org/0000-0001-9752-270X (2018) Process modelling and analysis of intensified CO2 capture using monoethanolamine (MEA) in rotating packed bed absorber. Journal of Cleaner Production, 204. pp. 1124-1142. ISSN 0959-6526

https://doi.org/10.1016/j.jclepro.2018.09.089

Process modelling and analysis of intensified CO_2 capture using monoethanolamine (MEA) in rotating packed bed absorber

Tohid Nejad Ghaffar Borhani[a], Eni Oko[a] and Meihong Wang[*a]

[a] Department of Chemical and Biological Engineering, The University of Sheffield, Sheffield S1 3JD, UK

Abstract

Rotating packed bed (RPB) absorber using monoethanolamine (MEA) as the solvent to capture CO_2 is modelled at steady state condition in this study according to the first principles in gPROMS®. The effect of eight different kinetic reaction models and five enhancement factors is examined based on the newly developed model. Selection of kinetic model has significant effect on the carbon capture level (CCL) but the effect of enhancement factor relation is not important. The steady state process model is validated against the experimental data and showed good agreement. The average absolute relative deviation for 12 case-runs is 3.5%. In addition, process analysis is performed to evaluate the effect of four factors namely rotor speed, MEA concentration in lean MEA solution, lean MEA solution temperature and lean MEA solution flow rate on CCL. Finally, orthogonal array design (OAD) method is applied to analyse the simultaneous effect of the above-mentioned factors in the CCL and motor power of RPB absorber by considering 25 scenarios. The result of using OAD revealed that rotor speed has the most important effect on CCL, and after that lean MEA solution flow rate has the second importance. In addition, the OAD method is used to find the proper combination of four factors that resulted in about 90% CCL with low motor power.

Keywords: Carbon capture, Chemical absorption, Process intensification, Rotating packed bed, Process modelling, Orthogonal array design.

Nomenclature

A_c	Cross sectional area which is 2πrz for RPB (m^2)
a_{gl}	Gas-liquid interfacial area (m^2/m^3)
a_p	Total surface area of packing (m^2/m^3)
a_w	Wetted surface area of packing (m^2/m^3)
C_{l,CO_2}^I	The interfacial liquid side concentration of CO_2 at equilibrium with gas phase
$C_{l,i}$	Molar concentration of component i in lean MEA solution (M≡kmol/m^3)

* Corresponding author.
E-mail address: meihong.wang@sheffield.ac.uk (Professor Meihong Wang)
Tel.: +44(0)1142227160

$C_{pg,i}$	Specific heat capacity of component i in gas phase(J/(kmol.K))
C_{pg}	Specific heat capacity of gas phase (J/(kmol.K))
$C_{pl,i}$	Specific heat capacity of component i in lean MEA solution (J/(kmol.K))
C_{pl}	Specific heat capacity of lean MEA solution (J/(kmol.K))
d_p	Effective diameter of packing (m) ($d_p = 6(1-\varepsilon)/a_t$)
$D_{g,ave}$	Average diffusivity in gas phase (m^2/s)
$D_{g,i}$	Diffusivity of component i in gas phase (m^2/s)
$D_{g,i-j}$	Gas phase diffusivity of component i in component j (m^2/s)
$D_{l,i}$	Diffusivity of component i in lean MEA solution (m^2/s)
$D_{l,i-j}$	Liquid phase diffusivity of component i in component j (m^2/s)
E_i	Enhancement factor of component i
$E_{n,m}$	Enhancement factor by using model number n in Table 3 and kinetic model number m in Table 2
F_g	Molar flow rate of gas phase (kmol/s)
F_l	Molar flow rate of lean MEA solution (kmol/s)
g_c	Centrifugal acceleration (m/s^2) ($g_c = r\omega^2$)
g_0	Characteristic acceleration (m/s^2) ($g_0 = 100$)
Ha	Hatta number
h_{gl}	Heat transfer coefficient ($W/(m^2.K)$)
$He_{l,i}$	Henry's constant of component i in lean MEA solution ($kPa.m^3/kmol$)
$He_{j,i}$	Henry's constant of component i in solvent j ($kPa.m^3/kmol$)
$H_{l,i}^{E}$	Excess Henry's constant of component i in lean MEA solution ($kPa.m^3/kmol$)
$k_{g,ave}$	Average mass transfer coefficient in gas phase (m/s)
$k_{g,i}$	Mass transfer coefficient of component i in gas phase (m/s)
$K_{g,i}$	Overall mass transfer coefficient of gas for component i ($kmol/(m^2.kPa.s)$)
$k_{l,i}$	Mass transfer coefficient of component i in lean MEA solution (m/s)
k_B	Reaction rate constant for any base that deprotonate the zwitterion ($m^3/(kmol.s)$)
k_r	Forward reaction rate constant ($m^3/(kmol.s)$)
k_{-r}	Backward reaction rate constant ($m^3/(kmol.s)$)
k_{obs}^{Z}	Observed reaction rate constant based on zwitterion mechanism (1/s)
k_{obs}^{T}	Observed reaction rate constant based on zwitterion mechanism (1/s)
k_i^T	Third order reaction rate constant for component i (MEA and H_2O) ($m^6/(kmol^2.s)$)
MV^*	Molar volume associated with the interaction between MEA and H_2O ($m^3/kmol$)
MW_i	Molecular weight of component i (kg/kmol)
MW_{ave}	Average molecular weight (kg/kmol)
N_i	Molar flux of component i ($kmol/(m^2.s)$)
P	Total pressure of gas phase (kPa)
P_i	Partial pressure of component i in the bulk gas (kPa)
P_i^*	Equilibrium partial pressure of component i corresponding to its concentration in the bulk liquid (kPa)
P_i^v	Vapor pressure of component i (kPa)
P_{motor}	Motor power (kW)
Q_g	Volumetric flow rate of gas phase (m^3/s)
Q_l	Volumetric flow rate of lean MEA solution (m^3/s)
Q_l'	Volumetric flow rate of lean MEA solution (L/min)
q_g	Heat transfer flux in gas phase (W/m^2)
q_l	Heat transfer flux in liquid phase (W/m^2)
$r_{CO_2}^{Z}$	Reaction rate of CO_2 with MEA based on zwitterion mechanism
$r_{CO_2}^{T}$	Reaction rate of CO_2 with MEA based on termolecular mechanism

R_i	The inner radius of RPB (m)
R_o	The outer radius of RPB (m)
R_g	Universal gas constant (kPa.m^3/(kmol.K))
T_g	Gas phase temperature (K)
$T_{g,0}$	Gas phase temperature in the inlet (K)
T_l	Liquid phase temperature (K)
$T_{l,0}$	Liquid phase temperature in the inlet (lean MEA solution temperature) (K)
u_g	Superficial gas velocity (m/s)
u_l	Superficial liquid velocity (m/s)
u_{l0}	Characteristic superficial flow velocity (m/s)
$V_{m,i}$	Molar volume of component i. (m^3/kmol)
V_m^*	Molar volume associated with the interaction between H_2O and MEA
x_i	Mole fraction of component i in liquid phase
x_0	Mole fraction of component i in lean MEA solution
y_i	Mole fraction of component i in gas phase
y_0	Mole fraction of component i in the inlet gas
Z	Axial height of the packing (m)

Greek Symbols

α_{CO_2}	CO_2 loading (mol CO_2/mol MEA)
α_{i-j}	The two body interaction parameter between components i and j
γ_i	Activity coefficient of component i
ε	Porosity of packing (m^3/m^3)
ε_L	Liquid hold-up
ϑ_i	Diffusion volume of component i
σ_c	Critical surface tension (N/m)
σ	Surface tension (N/m)
ρ_g	Density of gas phase (kg/m^3)
$\rho_{g,i}$	Density of component i in gas phase (kg/m^3)
ρ_l	Density of liquid phase (kg/m^3)
$\rho_{l,i}$	Density of component i in liquid phase (kg/m^3)
λ_g	Thermal conductivity of gas phase (W/(m.K))
μ_g	Dynamic viscosity of gas phase (Pa.s)
$\mu_{g,i}$	Dynamic viscosity of component i in gas phase (Pa.s)
μ_l	Dynamic viscosity of liquid phase (Pa.s)
$\mu_{l,i}$	Dynamic viscosity of component i in liquid phase (Pa.s)
υ_g	Kinematic viscosity of gas phase (m^2/s)
υ_l	Kinematic viscosity of liquid phase (m^2/s)
υ_{l0}	Characteristic kinematic viscosity of liquid phase (m^2/s)
ϕ_i	Volume fraction of component i in liquid solution
ω	Angular velocity (rad/s)
ΔP	Dry pressure drop for RPB (kPa)
ΔH_{CO_2}	Heat of absorption of CO_2 (J/kmol)
ΔH_{vap}	Heat of vaporization of H_2O (J/kmol)

Dimensionless groups

Fr_l	Froude number ($u_l^2 a_p / g_c$)
Gr_l	Grashof number of liquid phase ($d_p^3 g_c / v_g$)
Re_g	Reynolds number of gas phase ($u_g \rho_g / a_p \mu_g$)
Re_l	Reynolds number of liquid phase ($u_l \rho_l / a_p \mu_l$)
$Sc_{g,i}$	Schmidt number of component i in gas phase ($\mu_{g,i} / \rho_{g,i} D_{g,i}$)

$Sc_{l,i}$	Schmidt number of component i in liquid phase ($\mu_{l,i}/\rho_{l,i}D_{l,i}$)
We_l	Webber number ($u_l^2\rho_l/a_p\sigma$)
Abbreviations	
AARD	Average absolute relative deviation
AD	Absolute deviation
ARD	Average relative deviation
CCL	Carbon capture level
MEA	Monoethanolamine
$MEACOO^-$	Carbamate ion of MEA
$MEAH^+COO^-$	Zwitterion ion of MEA
OAD	orthogonal array design
PB	Packed bed
RPB	Rotating packed bed

1 Introduction

CO_2 needs to be removed from flue gas streams from power plants and industries due to its high contribution to global warming. There are different technologies to address this important issue (Arias et al., 2016). Among these technologies, chemical absorption using solvents is a promising method and many studies have been performed so far (Borhani et al., 2015). One of the most well-known chemical solvents, monoethanolamine (MEA), is considered as the benchmark solvent for CO_2 absorption (Liu et al., 2016). CO_2 capture using MEA is frequently carried out using packed beds (PBs) which is a widely used industrial units. In recent years, in addition to PB, another type of unit operation namely rotating packed beds (RPBs) has attracted significant attention (Wang et al., 2015). Therefore, some researchers tried to use RPB absorber instead of PB absorber for CO_2 capture application (Jassim et al., 2007; Joel et al., 2014).

The large size of the equipment (e.g. PBs and heat exchangers), high capital and operating costs, high energy consumption, and the possible necessity of having intercooling with heat integration have been mentioned as the challenges of PB systems. Using RPBs instead of PBs have some advantages: (a) considerable increase in the mass transfer rate (by increasing interfacial area due to droplet and film flow achieved by centrifugal acceleration) leading to significant reduction in size and weight of the rigs; (b) reduction in energy consumption; (c) wider flooding limit; (d) due to the short residence time in RPB, this system is proper for cases that require short contact time such as selective absorption of H_2S in the presence of CO_2 (Qian et al., 2010). Driven by these mentioned advantages, it is highly valuable to have high-quality research (through experiments and modelling) on CO_2 capture in RPB absorber

and stripper. Modelling of RPB system will be helpful in scale-up, optimization, troubleshooting, optimum design and process analysis. By removing carbon dioxide from different gas streams from power plants and chemical/process manufacturing, the human will be able to have cleaner productions and prevent global warming. The current study addresses development of a more compacted absorber for CO_2 capture which is within the theme of the cleaner productions. Studies in the literature have shown that substituting PBs with RPBs could lead to significant foot-print reduction of the post-combustion CO_2 capture process. gPROMS® is utilized as the platform in this study, since the physical property models/correlations, kinetic models, enhancement factor, and other important parameters that have significant effect on the model results can be selected by user and be modified if necessary in an object-oriented manner.

1.1 Review of previous studies on RPB absorber modelling

A few studies that focused on process modelling of RPB system are illustrated in Table 1. In comparison to PB systems, there are considerably less number of modelling and experimental studies on using RPB for CO_2 absorption.

Table 1: List of modelling studies on RPB absorber and stripper for CO_2 capture.

Reference	Platform	Validation	Solvent	Concentration	Description
Yi et al. (2009)	MTALAB®	Own data	DEA-K_2CO_3	4 wt.%+27 wt.%	Absorber steady-state model. Examining the effect of some parameters on overall mass transfer coefficient.
Qian et al. (2009)	FORTRAN®	Own data	MDEA	10-30 wt.%	Absorber steady-state model. The authors used Higbie's penetration theory. They examined the effect of rotor speed on mole fraction of CO_2 in outlet gas and liquid side mass transfer coefficient
Yu et al. (2012)	Unknown	Own data	DETA MEA DETA-PZ MEA-PZ	30 wt.% 30 wt.% 20 wt.%+10 wt.% 20 wt.%+10 wt.%	Absorber steady-state model using six stirred tanks in series
Kang et al. (2014)	gPROMS®	(Yu et al., 2012) (Jassim et al., 2007)	MEA	30 wt.% 30, 55, 75 wt.%	Absorber steady-state model. Examining the effect of different mass transfer coefficients and process analysis
Joel et al. (2014)	ASPEN PLUS® + FORTRAN®	(Jassim et al., 2007)	MEA	55, 75 wt.%	Absorber steady-state simulation and process analysis. The authors used visual FORTRAN® as subroutines and then dynamically linked to ASPEN PLUS®
Joel et al. (2015)	ASPEN PLUS® + FORTRAN®	(Jassim et al., 2007)	MEA	55, 75 wt.%	Absorber steady-state simulation and comparison of the effect of different mass transfer coefficient correlations
Kang et al. (2016)	gPROMS®	Own data (Jassim et al., 2007)	NH_3 MEA	3 wt.% 30 wt.%	Absorber steady-state model for comparison between PB and RPB

Joel et al. (2017)	ASPEN PLUS® + FORTRAN®	(Jassim et al., 2007) (Cheng et al., 2013)	MEA	30-55 wt.% 30 wt.%	Stripper steady-state simulation and process analysis

According to Table 1, Yi et al. (2009) studied the CO_2 absorption using DEA-potassium carbonate solution. The model was developed in MATLAB® with a few information about the physical properties utilized in the study. Higbie's penetration theory is utilized to perform steady-state RPB absorber modelling in FORTRAN® using MDEA solution (Qian et al., 2009). As the model is based on penetration theory, the model equations and its approach are completely different from two film theory model. Yu et al. (2012) utilized six stirred tanks to model the RPB absorber. The benefit of this approach is the simplification of modelling process but maybe the assumption makes the problem far away from reality. Kang et al. (2014 and 2015) modelled the RPB absorber in gPROMS®. Joel et al. (2014, 2015, and 2017) simulated RPB absorber and stripper in ASPEN PLUS® by using FORTRAN® routines to insert some correlations that were not available in ASPEN PLUS®. The results of these studies are valuable and different aspects of RPB system were studied. So far, Henry constant and liquid diffusivity correlations used in existing models are for 30 wt% MEA solution. In addition, due to lack of kinetic models for concentrated MEA solution (>30 wt%), existing kinetic models need to be compared to identify the best model for predicting CO_2-MEA kinetics. Current studies do not address this problem.

1.2 Novel contributions of this study

In this study, rate-base mass transfer with enhancement factor was considered to model the RPB absorber. The rate-based model is developed to represent the absorption process of CO_2 in the concentrated MEA solution in the RPB. Physical property models and correlations valid for high concentration MEA solution are applied. The authors tried to give accurate information about all the utilized correlations, assumptions and methods. The novelties of the current study are: (a) the impact of using eight different kinetic models on the prediction of CCL is evaluated. Five different enhancement factor relations are utilized to evaluate the effect of these kinetic models. No such comparison has, to the best of the authors' knowledge, been investigated in the literature for RPB absorber; (b) the effect of using three liquid side mass transfer coefficients on enhancement factor is investigated; (c) after

validation of the model using experimental data from literature, process analysis is performed to find the effect of different operating factors on the CCL. The process analysis is done by considering different and comprehensive scenarios of changing rotor speed, MEA concentration in lean MEA solution, lean MEA solution temperature, and lean MEA solution flow rate; (d) multivariable sensitivity analysis through OAD method is performed by considering simultaneous effect of four factors.

2 Model development

The main assumptions for developing the steady state first principle model in this study include:

- The gas phase consists of CO_2, H_2O and N_2.
- The liquid phase consists of CO_2, H_2O, MEA and ionic species namely HCO_3^-, CO_3^{2-}, OH^-, H_3O^+, $MEAH^+$ and $MEACOO^-$.
- Only mass transfer flux of CO_2, H_2O, N_2 and MEA is considered and the mass transfer flux of ionic species is assumed to be zero.
- The gas phase is assumed to be ideal.
- The system is at steady state condition.
- Fluids flow only in radial direction.
- All the reactions occur only in the liquid film, and there is not any end effect in the system.
- The fluids contact between liquid and gas is counter current. The gases come from outer side to the centre and liquid flows from the centre to outside of the RPB.

In the following subsections, the main governing equations, rate equations, the effect of chemical reactions, equilibrium calculation and correlations/relations used to calculate physical and other properties required in the model are described in detail.

2.1 Main equations

In RPB, it can be assumed that the main change in concentration of components takes place in the radial direction. Therefore, the only radial direction is considered in the governing equations. Material and energy balances for the gas and liquid phases with their boundary conditions are as follows (Harun et al., 2012):

$$\frac{\partial(F_g y_i)}{\partial r} = a_{gl} N_i A_c \qquad B.C.: \begin{cases} \text{at } r = R_o : y_i = y_0 \\ \text{at } r = R_i : \dfrac{\partial(F_g y_i)}{\partial \mathrm{r}} = 0 \end{cases} \tag{1}$$

$$\frac{\partial(F_l x_i)}{\partial r} = a_{gl} N_i A_c \qquad B.C.: \begin{cases} \text{at } r = R_i : x_i = x_0 \\ \text{at } r = R_o : \dfrac{\partial(F_l x_i)}{\partial \mathrm{r}} = 0 \end{cases} \tag{2}$$

$$\frac{\partial(F_g C_{pg} T_g)}{\partial r} = a_{gl} q_g A_c \quad B.C.: \begin{cases} \text{at } r = R_o : T_g = T_{g,0} \\ \text{at } r = R_i : \dfrac{\partial(F_g C_{pg} T_g)}{\partial \mathrm{r}} = 0 \end{cases} \tag{3}$$

$$\frac{\partial(F_l C_{pl} T_l)}{\partial r} = a_{gl} q_l A_c \quad B.C.: \begin{cases} \text{at } r = R_i : T_l = T_{l,0} \\ \text{at } r = R_o : \dfrac{\partial(F_l C_{pl} T_l)}{\partial \mathrm{r}} = 0 \end{cases} \tag{4}$$

2.2 Rate equations

The mass transfer flux (N_i) is calculated based on the two-film theory which is widely used in the modelling of CO_2 absorption in different types of absorbers (Afkhamipour and Mofarahi, 2013; Borhani et al., 2016). This is obtained using the overall mass transfer coefficient and the difference between the partial pressures (as driving force) as follows (Kvamsdal et al., 2009):

$$N_i = K_{g,i}(P_i - P_i^*) \tag{5}$$

where P_i (kPa) is the partial pressure of component i in the gas phase and P_i^* (kPa) is the equilibrium partial pressure of component i corresponding to its concentration in the bulk liquid. $K_{g,i}$ is the overall gas phase mass transfer coefficient of component i and is calculated using the following relation (Kvamsdal et al., 2009):

$$\frac{1}{K_{g,i}} = \frac{R_g T_g}{k_{g,i}} + \frac{He_{l,i}}{E_i k_{l,i}} \tag{6}$$

The right-hand side term ($R_g T_g / k_{g,i}$) is the gas phase resistance and the second term ($He_{l,i}/E_i k_{l,i}$) is the liquid phase resistance. $k_{g,i}$ is the gas side mass transfer coefficient of component i, $k_{l,i}$ is the liquid side mass transfer coefficient of component i, E_i is the enhancement factor that accounted for the effect of chemical reaction on the model for component i, and $He_{l,i}$ is the Henry's constant for insoluble gases (CO_2 and N_2) in the liquid phase. As mentioned before, i is CO_2, H_2O, N_2 and MEA. As N_2 is an inert gas, its mass transfer can be ignored. It is also assumed that the resistance to mass transfer for water and MEA in the liquid phase is negligible. Then for water and MEA, the second term ($He_{l,i}/E_i k_{l,i}$) can

be eliminated. Therefore, the following relations are considered for mass transfer rate (Kvamsdal et al., 2009):

$$N_{MEA} = \frac{k_{g,MEA}}{R_g T_g}(P_{MEA} - P^*_{MEA}) \quad (7)$$

$$N_{H_2O} = \frac{k_{g,H_2O}}{R_g T_g}\left(P_{H_2O} - P^*_{H_2O}\right) \quad (8)$$

$$N_{CO_2} = \frac{1}{\frac{R_g T_g}{k_{g,CO_2}} + \frac{He_{l,CO_2}}{E_{CO_2} k_{l,CO_2}}}\left(P_{CO_2} - P^*_{CO_2}\right) \quad (9)$$

In Eq. (7)-(9), P_i can be calculated using multiplication of y_i and the total pressure of gas phase (P). P_i^*, must be calculated using vapor-liquid equilibrium (VLE) calculations which will be described in Section 2.3. The heat transfer rates (q_g and q_l) are defined as follows (Harun et al., 2012):

$$q_g = h_{gl}\left(T_l - T_g\right) \quad (10)$$

$$q_l = h_{gl}\left(T_l - T_g\right) - \Delta H_{CO_2} N_{CO_2} - \Delta H_{vap} N_{H_2O} \quad (11)$$

where q_g and q_l are heat transfer rate for the gas and liquid phases, respectively. h_{gl} is heat transfer coefficient, T_l and T_g are liquid and gas phase temperature, ΔH_{CO_2} is the heat of reaction of CO_2 and ΔH_{vap} is the heat of vaporization of H_2O.

2.3 Chemical reactions and their effects

In reactive absorption, in addition to mass transfer, the chemical reaction has a substantial effect on the process and must be accounted in the model. In this study, the overall kinetic reaction is accounted for the film of liquid phase by using enhancement factor. This is due to the importance of the liquid phase mass transfer resistance in CO_2 capture studies (Harker et al., 2003).

2.3.1 Chemical reactions

When CO_2 is absorbed in an aqueous MEA solution, the following overall reaction is occurred (Luo et al., 2015):

$$CO_2 + 2MEA \rightleftarrows MEACOO^- + MEAH^+ \quad (12)$$

Reaction (12) can be interpreted by using two important mechanisms. According to zwitterion mechanism which is proposed by Caplow (1968) and latter revisited by Danckwerts (1979), the

zwitterion ion ($MEAH^+COO^-$) produces as an intermediate product by reaction between CO_2 and MEA (Ebadi Amooghin et al., 2017). This zwitterion undergoes deprotonation by a base (B) to form carbamate ($MEACOO^-$) (reaction (14)) (Moftakhari Sharifzadeh et al., 2016):

$$CO_2 + MEA \underset{k_{-r}}{\overset{k_r}{\rightleftharpoons}} MEAH^+COO^- \quad (13)$$

$$MEAH^+COO^- + MEA \xrightarrow{k_B} MEACOO^- + BH^+ \quad (14)$$

According to termolecular mechanism which is proposed by Crooks and Donnellan (1989) and discussed by da Silva and Svendsen (2004), one MEA molecule has reaction with one molecule of CO_2 and one molecule of a base, simultaneously:

$$CO_2 + MEA \ldots MEA \rightleftharpoons MEACOO^- \ldots MEAH^+ \quad (15)$$

2.3.2 Reaction kinetics

Reaction (12) which is the overall reaction between CO_2 and MEA, can be described based on the two above mentioned mechanisms namely zwitterion (Eq. 14) and termolecular (Eq. 15) according to the following simplified relations (Luo et al., 2015; Vaidya and Kenig, 2007):

$$r_{CO_2}^Z = k_{obs}^Z C_{l,CO_2} = k_r C_{l,MEA} C_{l,CO_2} \quad (16)$$

$$r_{CO_2}^T = k_{obs}^T C_{l,CO_2} = (k_{MEA}^T C_{l,MEA} + k_{H_2O}^T C_{l,H_2O}) C_{l,MEA} C_{l,CO_2} \quad (17)$$

where $r_{CO_2}^Z$ and $r_{CO_2}^T$ are reaction rates of CO_2 with MEA, and k_{obs}^Z and k_{obs}^T are observed reaction rate constant based on zwitterion and termolecular mechanism, respectively and k_r is the reaction rate constant. C_{l,CO_2}, $C_{l,MEA}$, and C_{l,H_2O} are the concentration of CO_2, MEA and water, respectively. There are different models for k_r, k_{MEA}^T, and $k_{H_2O}^T$ that are summarized in Table 2.

Table 2: Selected kinetic models for CO_2 absorption using MEA solution.

No	Mechanism	Formula	Valid condition		Reference
(1)	Zwitterion	$k_r = 4.14 \times 10^{11} \exp\left(-\frac{5399}{T_l}\right)$	MEA conc. Temp CO_2 loading	: 0.5-12 M : 298-323 K : NA	(Ying and Eimer, 2013)
(2)	Zwitterion	$k_r = 4.4 \times 10^{11} \exp\left(-\frac{5400}{T_l}\right)$	MEA conc. Temp CO_2 loading	: 0-3.2 M : 313 K : NA	(Versteeg et al., 1996)
(3)	Termolecular	$k_{MEA} = 4.61 \times 10^9 \exp\left(-\frac{4412}{T_l}\right)$	MEA conc. Temp	: 3-9 M : 293-333 K	(Aboudheir et al., 2003)

		$k_{H_2O} = 4.55 \times 10^6 \exp\left(-\frac{3287}{T_l}\right)$	CO_2 loading	: 0.1-0.49 mol/mol	
(4)	Zwitterion	$k_r = 3.376 \times 10^{12} \exp\left(-\frac{6018}{T_l}\right)$	MEA conc. Temp CO_2 loading	: 0.5-5 M : 293-343 K : unloaded liquid	(Luo et al., 2012)
(5)	Termolecular	$k_{MEA} = 8.07 \times 10^{12} \exp\left(-\frac{4503}{T_l}\right)$ $k_{H_2O} = 3.51 \times 10^9 \exp\left(-\frac{3055}{T_l}\right)$	MEA conc. Temp CO_2 loading	: 0.5-5 M : 293-343 K : unloaded liquid	(Luo et al., 2012)
(6)	Zwitterion	$k_r = 4.396 \times 10^9 \exp\left(-\frac{3693}{T_l}\right)$	MEA conc. Temp CO_2 loading	: 1-5 M : 298-343 K : 0-0.4 mol/mol	(Luo et al., 2015)
(7)	Termolecular	$k_{MEA} = 1.844 \times 10^{10} \exp\left(-\frac{4112}{T_l}\right)$ $k_{H_2O} = 2.064 \times 10^5 \exp\left(-\frac{1766}{T_l}\right)$	MEA conc. Temp CO_2 loading	: 1-5 M : 298-343 K : 0-0.4 mol/mol	(Luo et al., 2015)
(8)	Termolecular	$k_{MEA} = 2.003 \times 10^{10} \exp\left(-\frac{4742}{T_l}\right)$ $k_{H_2O} = 4.147 \times 10^6 \exp\left(-\frac{3110}{T_l}\right)$	MEA conc. Temp CO_2 loading	: 1-5 M : 298-343 K : 0-0.4 mol/mol	(Luo et al., 2015)

The most well-known reaction kinetic models presented by Hikita et al. (1977), Versteeg et al. (1996), and Horng and Li (2002) are limited to narrow ranges of temperature (278-308 K, 291-313 K, and 303-313 K, respectively) and MEA concentration (0.02-0.18 M, 0-3.2 M, and 0.1-0.5 M respectively). Hence, there is no guarantee that these models can be correctly extrapolated to the other conditions especially higher MEA concentration. Among the available rate constant models, the model presented by Aboudheir et al. (2003) is based on a wider temperature range, higher concentration of MEA and pre-loading of MEA solution with CO_2 and is presented based on termolecular mechanism. The authors also reported that pseudo first order assumption is not satisfactory and instead proposed a complex numerical solution for the kinetic model for absorption of CO_2 in aqueous MEA. They also reported that only termolecular mechanism could be used to explain all observed kinetic phenomena. The model presented by Ying et al. (2013) is for a wide range of concentration, initial pre-loading of MEA solution with CO_2 and temperatures, but by looking at their model, it can be found that their model is almost similar to Versteeg et al. (1996) in aspect of coefficients and values. Lou et al. (2012) used unloaded MEA solution which is not a proper assumption in the real cases. Luo et al. (2015) presented three types of kinetic models to perform numerical analysis of the absorption rate. They mentioned that pseudo first

order is an appropriate assumption at high amine concentrations, low CO_2 loadings, low CO_2 driving force, and low temperature. All eight kinetic models presented in Table 2 are examined in this study.

2.3.3 Enhancement factor

Enhancement factor is utilized to take into account the effect of chemical reactions on the mass transfer in the model. These factors can be calculated using two different methods: by fitting experimental results and by theoretical derivation using some simplified assumptions for the model (Kale et al., 2013). In general, the enhancement factors depend on the reaction type (reversible or irreversible), the chemical kinetics, liquid composition, physical and transport properties of the components in the liquid, the reaction order and stoichiometry, and the mass transfer model (van Swaaij and Versteeg, 1992). Usually, the slowest or kinetically controlled reaction is considered for the enhancement factor determination. In CO_2 absorption process, the liquid phase mass transfer resistance is important and therefore enhancement factor should be used (Putta et al., 2017). In this study, five different relations of enhancement factor are considered to examine its effect on the CCL (see Table 3).

Table 3: Different Enhancement Factor relations.

No	Formula	Description	Reference
1	$E_{CO_2} = Ha = \frac{\sqrt{k_{obs} D_{l,CO_2}}}{k_{l,CO_2}}$	The pseudo first order reaction regime enhancement factor	(Danckwerts, 1970)
2	$E_{CO_2} = 1 + \frac{1}{\left[\left(\frac{1}{E_i - 1}\right)^{1.35} + \left(\frac{1}{E_1 - 1}\right)^{1.35}\right]^{\frac{1}{1.35}}}$	Explicit form second order reactions	(Wellek et al., 1978)
3	$E_{CO_2} = 1 + (E_2 - 1)\left[1 - \exp\left[-\frac{Ha - 1}{E_2 - 1}\right]\right]$	Explicit form second order reactions	(Porter, 1966)
4	$E_{CO_2} = \frac{\sqrt{(Ha)^2 \frac{E_i - E_{CO_2}}{E_i - 1}}}{\tanh\left(\sqrt{(Ha)^2 \frac{E_i - E_{CO_2}}{E_i - 1}}\right)}$,	Implicit form second order reactions	(van Krevelen and Hoftijzer, 1948)
5	$E_{CO_2} = \frac{E_1^2}{2(E_i - 1)}\left(\sqrt{1 + \frac{4(E_i - 1)E_i}{E_1^2}} - 1\right)$	Explicit form second order reactions	(Yeramian et al., 1970)

where

$$Ha = \frac{\sqrt{k_{obs} D_{l,CO_2}}}{k_{l,CO_2}}, E_i = 1 + \frac{D_{l,MEA} C_{l,MEA}}{2 D_{l,CO_2} C^I_{l,CO_2}}, \quad (18)$$

$$E_1 = \frac{Ha}{\tanh(Ha)}\ , E_2 = \sqrt{\frac{D_{l,CO_2}}{D_{l,MEA}}} + \sqrt{\frac{D_{l,MEA}}{D_{l,CO_2}}}\left(\frac{C_{l,MEA}}{2C^I_{l,CO_2}}\right)$$

It must be mentioned that the default kinetic model and enhancement factor relation for the model calculations are kinetic model number 8 and enhancement factor number 2. Kinetic model number 8 and enhancement factor number 2 are selected because they resulted in better prediction in terms of CCL and showed better agreement of experimental and predicted values.

2.4 Equilibrium calculations

Two important equilibrium calculations that are utilized in this studies are chemical and physical equilibrium. In the following sub sections these two type of calculations are described by details.

2.4.1 Chemical equilibrium

Chemical equilibrium, which is also well-known as speciation equilibrium, provides the concentration of different species in the solution. The well-known non-iterative and simple method, originally presented by Danckwert (1970), revisited by Gabrielsen et al. (2005), and applied in some researches (Llano-Restrepo and Araujo-Lopez, 2015), is utilized in this study.

2.4.2 Vapour-liquid equilibrium

In VLE calculations the chemical potential of both liquid and gas phases must be equal. In general there are two main approaches to perform VLE calculations namely homogenous approach (also well-known as ϕ-ϕ approach) in which one thermodynamic model is utilized to perform the calculation for both phases and heterogeneous approach (also well-known as γ-ϕ approach) in which one activity coefficient based thermodynamic model is utilized to perform liquid phase calculations and one equation of state (EOS) for gas phase calculations (Barreau et al., 2006). In addition to the main approaches, there is another method which is an empirical technique and is utilized by different researchers (Weiland et al., 1982). Heterogeneous approach is utilized in current study. Therefore, the following equations are considered for VLE calculations:

$$P_i^* = \gamma_i x_i P_i^v \quad i\text{= MEA and } H_2O \tag{19}$$

$$P^*_{CO_2} = \gamma_{CO_2} C_{l,CO_2} He_{l,CO_2} \quad (20)$$

where P_i^v is vapour pressure of component i and calculated using Extended Antoine equation. γ_i is the activity coefficient of component i predicted by Wilson model. C_{l,CO_2} is the molar concentration of free CO_2 in solution, and calculated using speciation equilibrium calculation. He_{l,CO_2} is the Henry's constant.

2.5 Correlations and methods for calculation of physical property and other parameters

The accuracy of the modelling results strongly depends on the proper selection of methods and correlations for the calculation of physical properties, mass and heat transfer coefficients, thermophysical, thermochemical, hydrodynamic effective interfacial area, and transport relations applied in the model. The list of these relations is provided in Table 4.

Table 4: Different types of methods and correlations utilized in current study.

Property	Formula/Symbol/Description	Reference
Gas Viscosity	μ_g	Multiflash package in gPROMS
Liquid Viscosity	$\mu_l = \mu_{l,H_2O} \exp \frac{[21.186\phi_{MEA}]\left[\alpha_{CO_2}(0.01015\phi_{MEA} + 0.0093T_l - 2.2589) + 1\right]\phi_{MEA}}{T_l^2}$	(Weiland et al., 1998)
Gas density	ρ_g	Multiflash package in gPROMS
Liquid density	$\rho_l = \frac{\sum_{i=1}^{n} x_i MW_i}{x_{MEA} x_{CO_2} V_m^* + \sum_{i=1}^{n} x_i V_{m,i}}$, $i = CO_2, MEA, H_2O$ $MV_i = \frac{MW_i}{\rho_{l,i}}$, $V_m^* = -1.8218 \times 10^{-3}, V_{m,CO_2} = 0.04747 \times 10^{-3}$	(Weiland et al., 1998)
	$\rho_{l,MEA} = 1.19093 - 4.2999 \times 10^{-4} T_l - 5.66040 \times 10^{-7} T_l^2$ $\rho_{l,H_2O} = 0.863559 - 1.21494 \times 10^{-3} T_l - 2.57080 \times 10^{-6} T_l^2$	(Hsu and Li, 1997)
Gas heat capacity	$C_{pg,CO_2} = 19795.19 + 73.436472 T_g - 0.056019 T_g^2 + 1.72 \times 10^{-5} T_g^3$ $C_{pg,H_2O} = 33738.11 - 7.0175634 T_g - 0.0272961 T_g^2 - 1.67 \times 10^{-5} T_g^3 + 4.30 \times 10^{-9} T_g^4 - 4.14 \times 10^{-13} T_g^5$ $C_{pg,MEA} = 13207.4 - 281.577 T_g - 0.1513066 T_g^2 + 3.13 \times 10^{-5} T_g^3$ $C_{pg,N_2} = 31149.792 - 13.565232 T_g - 0.02679552 T_g^2 - 1.17 \times 10^{-5} T_g^3$ $C_{pg} = \sum_{i=1}^{n} y_i C_{pg,i}$	(Harun, 2012)
Liquid heat capacity	$C_{pl,CO_2} = 78.2498 \times 10^3 + 293 T_l$ $C_{pl,MEA} = 96.317 - 124.1 T_l + 1.5981 \times 10^{-4} T_l^2 + 6.9827 \times 10^{-8} T_l^3$ $C_{pl} = \sum_{i=1}^{n} x_i C_{pl,i}$	(Agbonghae et al., 2014)

Gas side mass transfer	$k_{g,i} = 2(Re_g)^{0.7}(Sc_{g,i})^{1/3}\left(\frac{D_{g,i}}{a_p d_p^2}\right)$	(Onda et al., 1968)
Liquid side mass transfer	$k_{l,i} = 0.92\left(\frac{a_p}{a_{gl}}\right)^{1/3}(Re_l)^{1/3}(Sc_{l,i})^{1/2}(Gr_l)^{1/6}\left(\frac{D_{l,i}}{d_p}\right)$	(Tung and Mah, 1985)
	$k_{l,i} = 12\left(\frac{D_{l,i}}{d_p}\right)\left(\frac{\rho_l u_l}{\mu_l a_{gl}}\right)\left(\frac{\mu_l}{\rho_l D_{l,i}}\right)^{1/3}$	(Hanley and Chen, 2012)
	$k_{l,i} = 1.5\left(\frac{\rho_l g_c}{\mu_l}\right)^{1/6}\left(\frac{D_{l,i}}{d_p}\right)^{1/2}\left(\frac{u_l}{a_p}\right)^{1/3}$	(Billet and Schultes, 1999)
Interfacial area	$\frac{a_{gl}}{a_p} = 1 - \exp\left(-1.45\left(\frac{\sigma_c}{\sigma}\right)^{0.75} Re_l^{0.1} Fr_l^{-0.05} We_l^{0.2}\right)$	(Onda et al., 1968)
Henry's constant	$He_{l,CO_2} = He_{l,N_2O}\frac{He_{H_2O,CO_2}}{He_{H_2O,N_2O}}$ $He_{l,N_2O} = \exp(\phi_{MEA}\ln He_{MEA,N_2O} + \phi_{H_2O}\ln He_{H_2O,N_2O} + H^E_{l,N_2O})$ $He_{H_2O,CO_2} = 3.520\times10^6\exp\left(\frac{-2113}{T_l}\right)$ $He_{H_2O,N_2O} = 8.449\times10^6\exp\left(\frac{-2283}{T_l}\right)$ $He_{MEA,N_2O} = 2.448\times10^5\exp\left(\frac{-1348}{T_l}\right)$ $\phi_{MEA} = \frac{x_{MEA}V_{m,MEA}}{x_{MEA}V_{m,MEA} + x_{H_2O}V_{m,H_2O}}$ $\phi_{H_2O} = \frac{x_{H_2O}V_{m,H_2O}}{x_{MEA}V_{m,MEA} + x_{H_2O}V_{m,H_2O}}$ $H^E_{l,N_2O} = \phi_{MEA}\phi_{H_2O}\alpha_{MEA-H_2O}$	(Ying et al., 2012)
Liquid diffusivity	$D_{l,CO_2} = D_{l,N_2O}\frac{D_{l,CO_2-H_2O}}{D_{l,N_2O-H_2O}}$	Analogy
	$D_{l,N_2O} = \left(5.07\times10^{-6} - 3.5443\times10^{-7}C_{l,MEA} + 3.4294\times10^{-9}C_{l,MEA}^2\right)\exp\left(\frac{-2371 + 0.3749C_{l,MEA}}{T_l}\right)$	(Ying and Eimer, 2012)
	$D_{l,CO_2-H_2O} = 2.350\times10^{-6}\exp\left(\frac{-2119}{T_l}\right)$	(Versteeg and Van Swaaij, 1988)
	$D_{l,N_2O-H_2O} = 5.070\times10^{-6}\exp\left(\frac{-2371}{T_l}\right)$	(Versteeg and Van Swaaij, 1988)
	$D_{l,MEA-H_2O} = \exp\left(-13.275 - \frac{2198.3}{T_l} - 0.078142C_{l,MEA}\right)$	(Snijder et al., 1993)
	$D_{l,MEA} = D_{l,MEA-H_2O}\left(\frac{\mu_{l,H_2O}}{\mu_{l,MEA}}\right)^{0.6}$	(Versteeg and Van Swaaij, 1988)
	$D_{l,H_2O} = \frac{7.4\times10^{-8}(1.9\times MW_{MEA})^{0.5}T_l}{\mu_{l,MEA}V_{m,i}^{0.6}}$	(Wilke and Chang, 1955)
	$D_{l,N_2} = 10^{-7}$	(Harun et al., 2012)
Gas diffusivity	$D_{g,i} = \frac{1-y_i}{\sum_{j=1}^{n}(y_j/D_{g,i-j})}$	(Fairbanks and Wilke, 1950)
	$D_{g,i-j} = \frac{1.43\times10^{-7}T_g^{1.75}\left(\frac{1}{MW_i} + \frac{1}{MW_j}\right)^{0.5}}{P\times10^{-2}\left[(\sum\vartheta_i)^{\frac{1}{3}} - (\sum\vartheta_j)^{\frac{1}{3}}\right]^2}$	(Fuller et al., 1966)

Thermal conductivity	λ_g	Multiflash package in gPROMS
Pressure drop	$\Delta P = \frac{150(1-\varepsilon)^2\mu_g}{d_p^2\varepsilon^3}\left(\frac{Q_g}{2\pi Z}\right)\ln\left(\frac{R_o}{R_i}\right) + \frac{1.75(1-\varepsilon)\rho_g}{d_p\varepsilon^3}\left(\frac{Q_g}{2\pi Z}\right)^2\left(\frac{1}{R_i}-\frac{1}{R_o}\right)$ $+\frac{1}{2}\rho_g\omega^2(R_o^2-R_i^2) + \varepsilon\left(-0.08 + Q_g + (2000+\omega^{1.22})Q_g^2\right)$	(Llerena-Chavez and Larachi, 2009)
Liquid holdup	$\varepsilon_L = 0.039\left(\frac{g_c}{g_0}\right)^{-0.5}\left(\frac{u_L}{u_{L0}}\right)^{0.6}\left(\frac{\upsilon_l}{\upsilon_{l0}}\right)^{0.22}$, $g_c = r\omega^2, g_0 = 100\ \mathrm{m^2/s}, u_{L0} = 0.01\,\mathrm{m/s}, \upsilon_{l0} = 10^{-6}\ \mathrm{m^2/s}$	(Burns et al., 2000)
Heat transfer coefficient	$h_{gl} = k_{g,ave}R_gT_g\left(\frac{C_{pg}\rho_g}{MW_{ave}}\right)^{\frac{1}{3}}\left(\frac{\lambda_g}{D_{g,ave}}\right)^{\frac{2}{3}}$	(Chilton and Colburn, 1934)
Vapor pressure	P_i^v/Extended Antoine equation	(Harun, 2012)
Activity coefficient	γ_i/Wilson model	Multiflash package in gPROMS/(Prausnitz et al., 1998)

In literature, Henry's constant is commonly predicted using the N_2O analogy (Tsai et al., 2000; Versteeg and Van Swaaij, 1988; Wang et al., 1992). This approach has been used in CO_2 absorption models in literature (Harun et al., 2012; Kang et al., 2014). The Henry constant model presented by Ying et al. (2012) is valid for 0-100 wt.% MEA solution and temperature range of 298.15-323.15 K. It was realized that the Henry constant model of Ying et al. (2012) predicted the values with a better agreement to the experimental data. The diffusion coefficient model presented by Ying and Eimer (2012) is developed for MEA solution up to 12 M (71 wt.%) and temperature range of 298.15-333.15 K. The prediction of density and viscosity has been done using Weiland et al. (1998) correlation. This correlation, unlike other correlations in literature, accounts for CO_2 loading of aqueous MEA. It must be mentioned that all the models and correlations were validated against the experimental data.

2.6 Model solution

The model was implemented in gPROMS® Model Builder V4.2. SRADAU solver based on Second-order Centred Finite Difference Method (CFDM) is utilized to solve the equations of the model. These equations contain main governing ordinary differential equations and linear and non-linear algebraic equations for calculation of the different parameters, methods and correlations.

3 Model results and validation

Jassim (2002) presented experimental data for absorption of CO_2 in RPB absorber system using MEA solution for four different MEA concentrations of 30, 55, 75 and 100 wt.%. These data contain different operating conditions (temperature, pressure, rotor speed, and MEA concentrations). The characteristics of RPB absorber which are fixed for all runs and cases are illustrated in Table 5. The process conditions, which are utilized as inputs to the system in this study, can be found in Table 6. Experiments performed using the average concentrations of 55 wt.% and 75 wt.% MEA solutions are considered as Case 1 and Case 2, respectively. Six selected runs for each case are examined as input data to the model. The amount of CO_2 capture is employed to compare the predicted values from the developed model with the experimental data. CO_2 capture level (CCL) percent is computed according to the following relation:

$$\mathrm{CCL\%} = \left(\frac{\mathrm{y}_{\mathrm{CO_2}}^{\mathrm{in}} - \mathrm{y}_{\mathrm{CO_2}}^{\mathrm{out}}}{\mathrm{y}_{\mathrm{CO_2}}^{\mathrm{in}}}\right) \times 100 \tag{21}$$

In order to have better insight into the model predictions, some error analysis was used in this study. The relation of absolute relative deviation (ARD %) reflecting the comparison of the experimental and predicted CCL and the relation of absolute deviation percent (AD%) presenting the comparison of the experimental and predicted mole fraction of CO_2 in the gas phase are as follows:

$$\mathrm{ARD\%} = \left|\frac{\mathrm{CCL}^{\mathrm{Exp}} - \mathrm{CCL}^{\mathrm{Pre}}}{\mathrm{CCL}^{\mathrm{Exp}}}\right| \times 100 \tag{22}$$

$$\mathrm{AD\%} = \left|\mathrm{y}_{\mathrm{CO_2}}^{\mathrm{Exp}} - \mathrm{y}_{\mathrm{CO_2}}^{\mathrm{Pre}}\right| \times 100 \tag{23}$$

where $\mathrm{y}_{\mathrm{CO_2}}^{\mathrm{in}}$ and $\mathrm{y}_{\mathrm{CO_2}}^{\mathrm{out}}$ are inlet and outlet mole fractions of CO_2 in the gas phase, respectively. $\mathrm{y}_{\mathrm{CO_2}}^{\mathrm{Exp}}$ and $\mathrm{y}_{\mathrm{CO_2}}^{\mathrm{Pre}}$ are experimental and predicted mole fractions of CO_2 at outlet.

Table 5: The RPB absorber characteristics (Jassim et al., 2007).

Parameter	Values
Rotor speed (rpm)	600, 1000
Diameter of RPB (m)	0.398 (OD), 0.156 (ID)
Porosity of packing (m^3/m^3)	0.76
Packing type	Expanded stainless steel small mesh
Packing height (m)	0.025
Total surface area (a_t) (m^2/m^3)	2132

Table 6: Process conditions as input to the RPB absorber (Jassim, 2002).

MEA	Case-Run	Rotor Speed	Pressure	Flow rate		Temperature		Liquid mole fraction			Gas mole fraction		
wt.%		rpm	atm	liquid (l/min)	gas (kmol/h)	gas in (˚C)	liquid in (˚C)	H_2O	CO_2	MEA	H_2O	CO_2	N_2
56.0	1-1	600	1	39.3	2.87	47	39.6	0.6970	0.0216	0.2814	0.1679	0.0471	0.7850
53.2	1-2	600	1	39.3	2.87	47	20.7	0.7171	0.0234	0.2595	0.1690	0.0460	0.7850
56.0	1-3	1000	1	39.3	2.87	47	40.1	0.6970	0.0216	0.2814	0.1702	0.0448	0.7850
55.0	1-5	600	1	21.1	2.87	47	39.5	0.6967	0.0277	0.2756	0.1707	0.0443	0.7850
56.0	1-6	600	1	21.1	2.87	47	22.3	0.6890	0.0274	0.2836	0.1703	0.0447	0.7850
55.0	1-7	1000	1	21.1	2.87	47	39.6	0.6969	0.0276	0.2755	0.1715	0.0435	0.7850
77.0	2-2	600	1	39.3	2.87	47	21.4	0.4688	0.0200	0.5112	0.1714	0.0436	0.7850
74.0	2-3	1000	1	39.3	2.87	47	40.2	0.5057	0.0229	0.4714	0.1714	0.0436	0.7850
75.1	2-4	1000	1	39.3	2.87	47	20.7	0.5008	0.0169	0.4823	0.1721	0.0429	0.7850
76.0	2-6	600	1	21.1	2.87	47	22.1	0.4795	0.0221	0.4984	0.1712	0.0438	0.7850
75.0	2-7	1000	1	21.1	2.87	47	39.4	0.4876	0.0256	0.4868	0.1712	0.0438	0.7850
78	2-8	1000	1	21.1	2.87	47	20.6	0.4515	0.0215	0.5270	0.1697	0.0453	0.7850

In Table 7, the experimental and the predicted CO_2 capture levels are compared for twelve selected case-runs. The comparison reveals that there is a good agreement between these values. ARD% between the experimental and the predicted CCLs is in the range of 0.79 to 6.97 which is reasonable and acceptable error range in engineering applications and is comparable with the experimental results presented by Jassim (2002). The average absolute relative deviation (AARD %) for all the twelve case-runs is 3.5% that indicates the model has reasonable and trustable ability to predict the CCLs. In addition, AD% between the experimental and the model predicted CO_2 mole fractions in the gas phase is changing from 0.03 to 0.26 which show the strength of model to predict these values accurately. The average absolute deviation (AAD %) for twelve case-runs is about 0.14.

Table 7: Model prediction results compared to the experimental values.

Case	Run	Exp. CO_2 capture level %	Pre. CO_2 capture level %	ARD% between Exp. & Pre. CCL	AD% between Exp. & Pre. y_{CO_2}
1	1	94.9	90.98	4.13	0.18
1	2	83	86.86	4.65	0.18
1	3	95.4	97.58	2.28	0.10
1	5	87	88.77	2.03	0.08
1	6	84.1	84.95	1.01	0.04
1	7	89.9	93.41	3.90	0.15
2	2	84.2	90.06	6.97	0.26
2	3	97.5	98.54	1.07	0.05
2	4	91.2	97.05	6.41	0.25
2	6	84.3	87.20	3.45	0.13
2	7	98.1	97.32	0.79	0.03
2	8	91	95.88	5.36	0.22

The CO_2 mole fraction profiles for different cases and runs are illustrated in Figure 1. It must be mentioned that in this figure the mass transfer coefficient correlation presented by Tung and Mah (1985) is utilized. As can be seen all the cases show the same trend inside the RPB. The outer radius where flue gas enters to the RPB is the point that has the highest amount of CO_2 in the flue gas and the gas stream by passing the radius of RPB loss its CO_2.

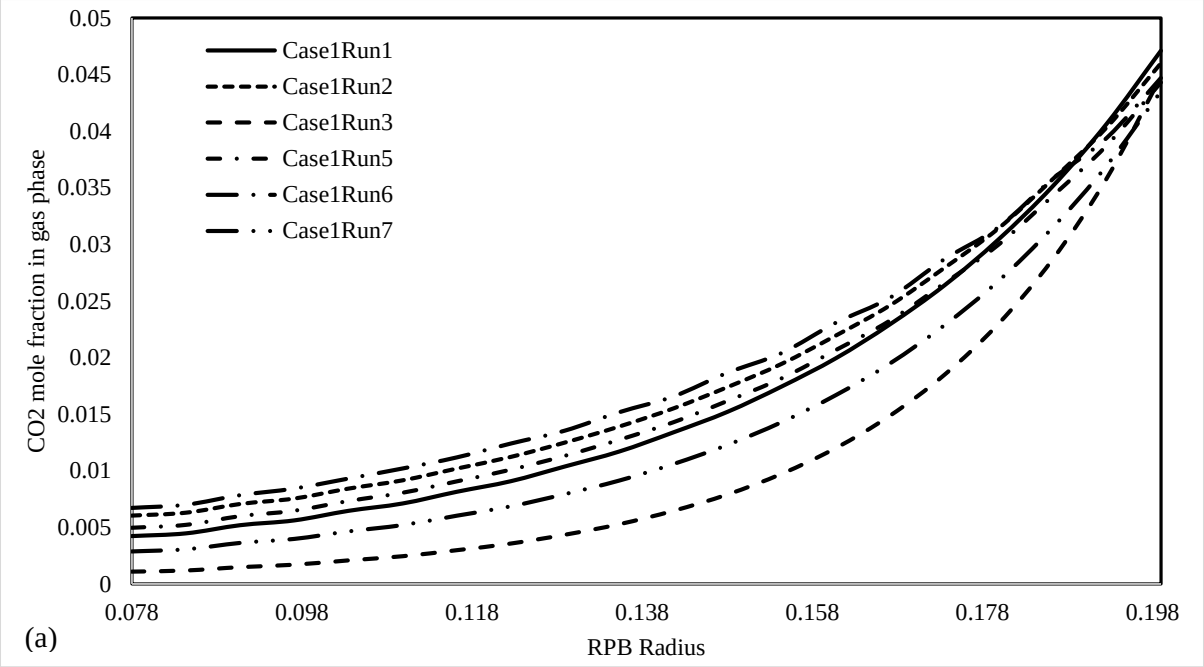

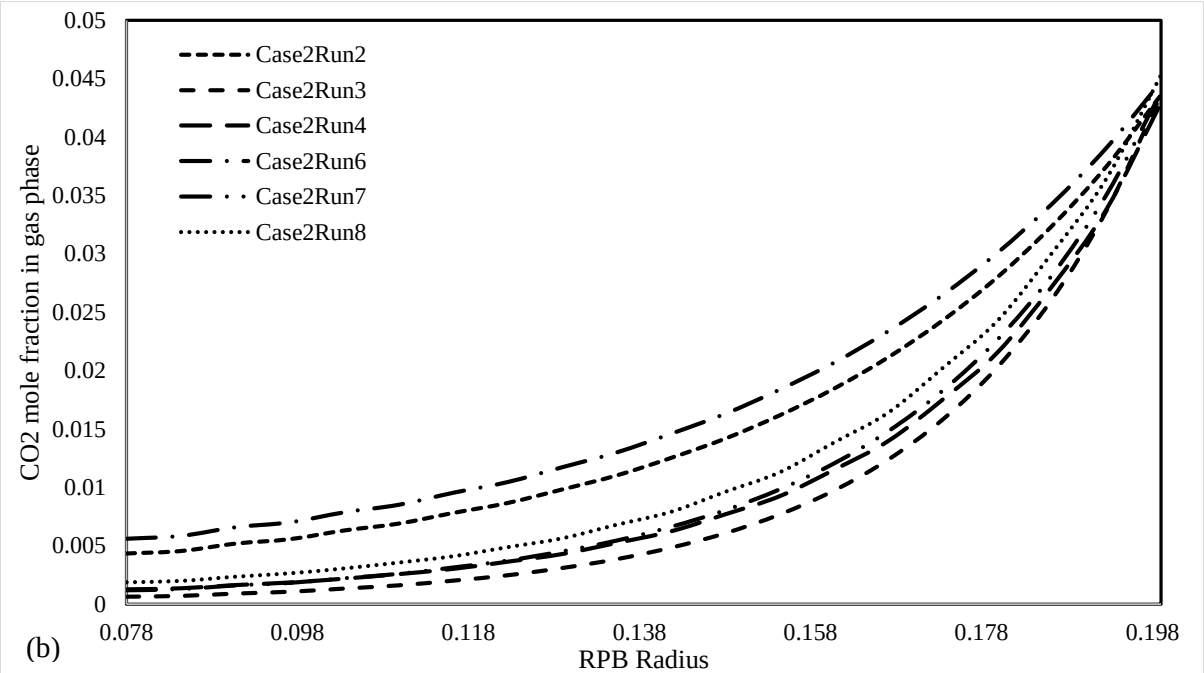

Figure 1: The profile of CO_2 in the RPB for (a) MEA concentration 53-57 wt.% and (b) MEA concentration 72-78 wt.%.

4 Effects of kinetic reaction and enhancement factor on model

Prediction of the rate constant for the reaction between CO_2 and MEA solution by using different kinetic relations presented in Table 2 is illustrated in Figure 2 for two different MEA wt.% reported in the experimental data (case 1 run 5 and case 2 run 3).

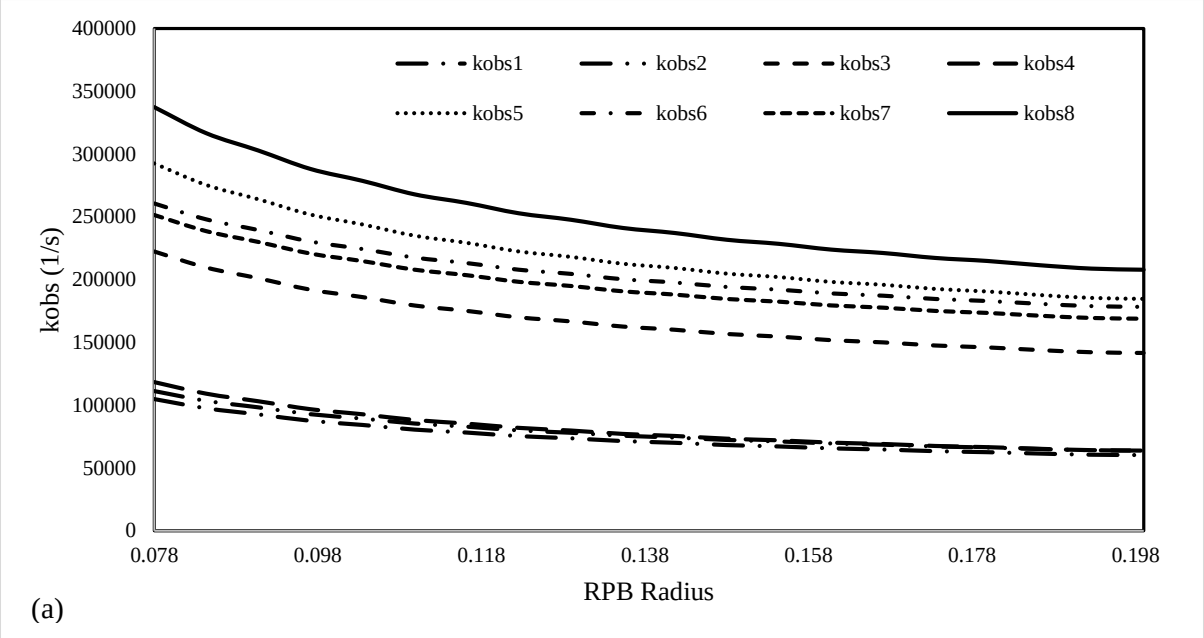

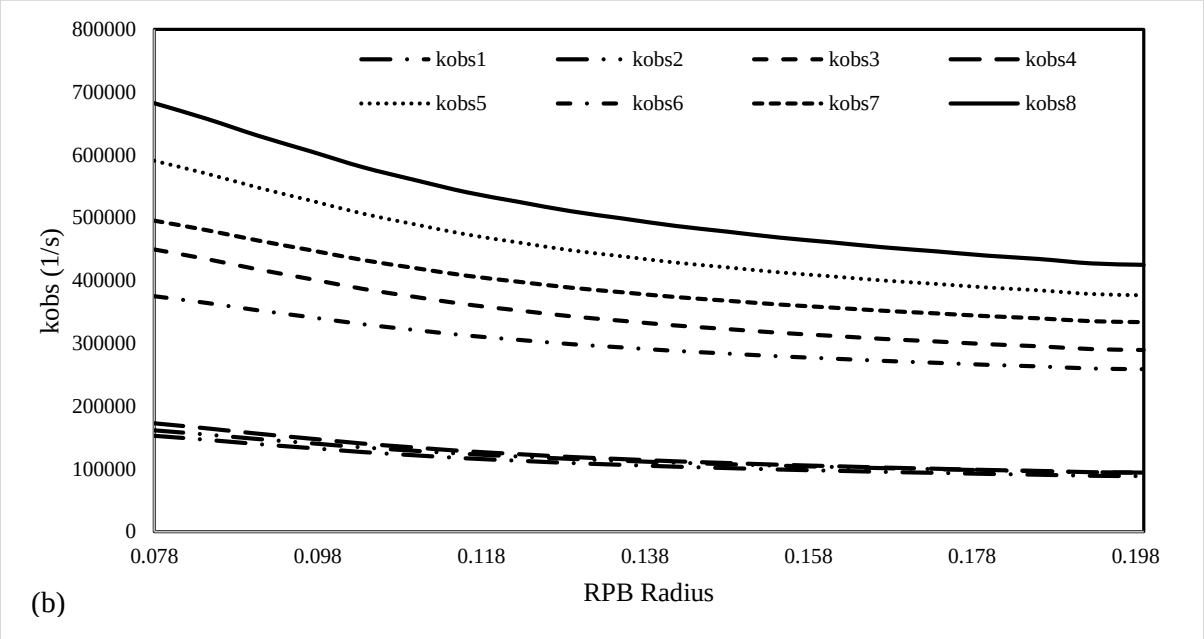

Figure 2: Change of reaction rate through radial direction of RPB for (a) for 55 wt.% MEA solution (case 1 run 5) and (b) for 74 wt.% MEA solution (case 2 run 3).

As can be seen in both MEA concentrations, models 1, 2 and 4 in Table 2 predicted the k_{obs} less than the other models. This underestimation has a negative effect on the enhancement factor, and, consequently, on the CO_2 capture of the model. Among the kinetic models, model 8 has the highest value of kinetic reaction rate, and, therefore, the highest CO_2 capture is obtained by using this model. It is also clear that models 1, 2 and 4 do not reflect the effect of MEA concentration. This means that these models are not proper for the higher concentration range of amine, and cannot be extrapolated to

the other conditions (Faramarzi et al., 2010). In contrast, the models 8 and 7 showed that they can effectively account for the effect of MEA concentration. In order to have a better insight on the selection of kinetic model, the average value of k_{obs} for case 1 run 5 and case 2 run 3 are presented in Table 8. The values of observed reaction rate constant are different considerably which these values have direct effect on the CCL prediction of the model. As can be seen the value predicted by k_{obs8} in both cases is higher than the other kinetic models. In addition, the value of observed reaction rate constant predicted by models 1, 2 and 4 are in the same range.

Table 8: Average value of the observed reaction rate constant.

MEA wt. %	k_{obs1}	k_{obs2}	k_{obs3}	k_{obs4}	k_{obs5}	k_{obs6}	k_{obs7}	k_{obs8}
55 (case 1 run 5)	74506	78928	168008	80864	219718	205574	195957	249800
74 (case 2 run 3)	110908	117491	346078	121167	452343	300530	391575	515844

The effect of using different liquid side mass transfer coefficients on pseudo first order enhancement factor (relation number 1 in Table 3) is illustrated in Figure 3. Figure 3 (a) shows the effect of using Tung and Mah (1985) liquid side mass transfer coefficient model. As can be seen profiles of all kinetic models are smooth and consistent. Figure 3 (b), which is the profile of enhancement factor by using Hanley and Chen (2012) liquid side mass transfer coefficient show slightly different behaviour and an increase of the enhancement factor from inner to outer radius of RPB. The biggest value of the enhancement factor is calculated using this mass transfer correlation. Figure 3 (c) is constructed by using Billet and Schultes (1999) resulted in the smallest value of the enhancement factor.

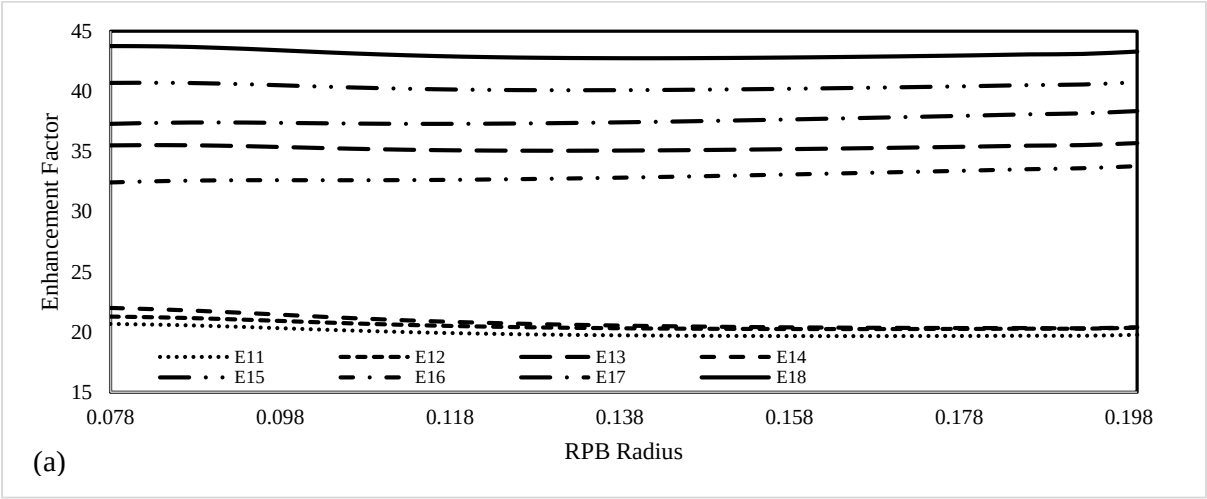

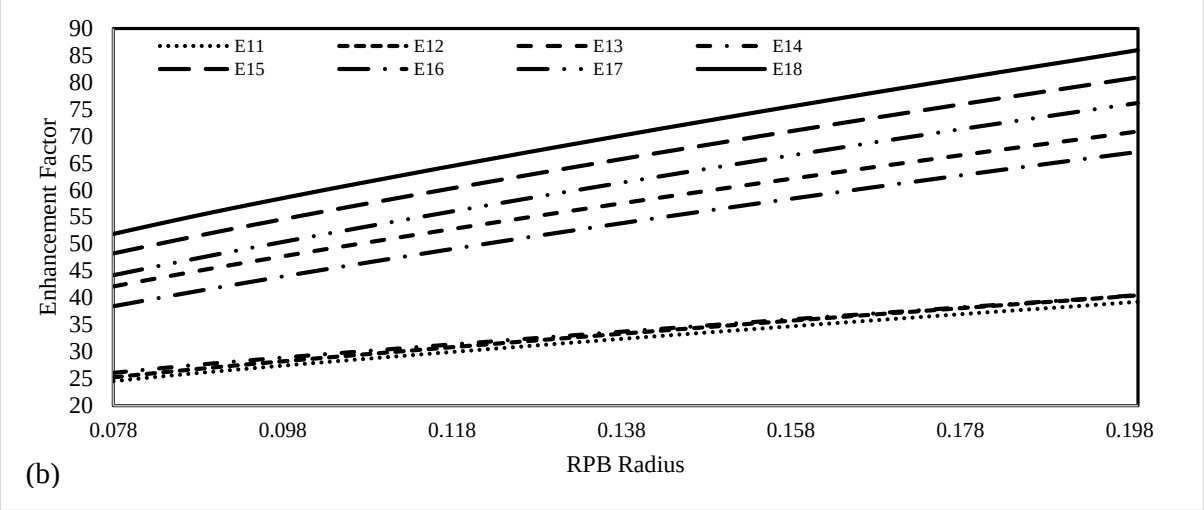

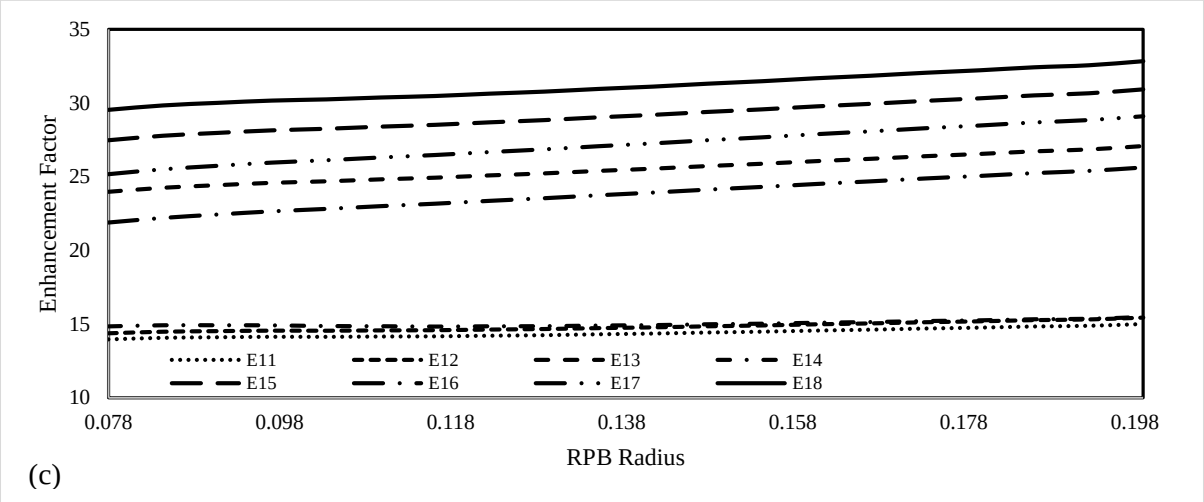

Figure 3: Effect of using different mass transfer coefficient on enhancement factor (a) by using Tung and Mah (1985), (b) by using Hanley and Chen (2012), (c) by using Billet and Schultes (1999).

It must be mentioned that $E_{n,m}$ is the enhancement factor by enhancement relation number n (in Table 3) and kinetic model by number m (in Table 2). Moreover, the effect of using different enhancement factor relations is examined by selecting kobs8 in Figure 4. It must be mentioned that the enhancement factor correlation presented by van Krevelen and Hoftijzer (1948) and Yeramian et al. (1970) (relations number 4 and 5 in Table 3) showed very near values.

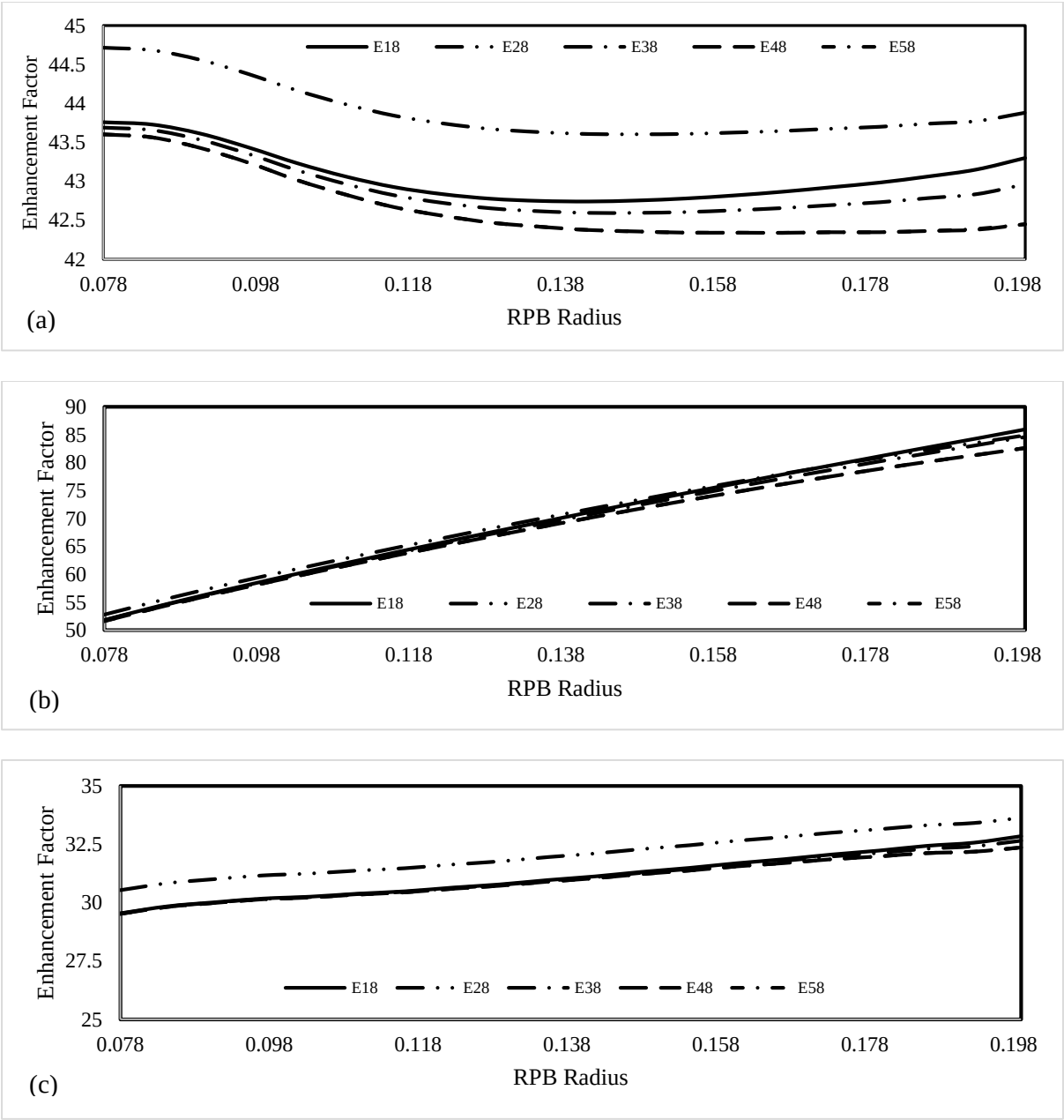

Figure 4: Effect of enhancement factor relation for kobs8 (a) by using Tung and Mah (1985), (b) by using Hanley and Chen (2012), (c) by using Billet and Schultes (1999).

According to Figure 4, the value of enhancement factor calculated by using different relations for kobs8 is higher than that of calculated by using relation presented by Wellek et al. (1978). For the other three models the amount of enhancement factor in inner radius of RPB is almost the same but there are some differences in the outer radius in which gas flue enter to the system, and, therefore, the effect of the chemical reaction is more significant. The Figure 4 also shows that amount of enhancement factor for kobs8 is considerably higher than kobs3.

The effect of using different enhancement factor relations is considered for case 1 run 1. The average value of enhancement factor for kobs8 and five enhancement factor is presented in Table 9.

Table 9: Average value of the enhancement factor calculated using different relations for kobs8.

E_{18}	E_{28}	E_{38}	E_{48}	E_{58}
27.97	28.82	27.86	27.65	27.67

where $E_{n,m}$ is the enhancement factor by enhancement relation number n (in Table 3) and kinetic model by number m (in Table 2). According to Table 9 the enhancement factor relation does not have significant effect on the value of enhancement factor and by using all the relations similar values can be obtained. It must be mentioned that Tung and Mah (1985) model is applied to calculate the mass transfer coefficient of the liquid phase in Table 9. Therefore, relied upon this study, it is clear that the kinetic reaction model is very important, and has significant effect on the final capture level but the relation of enhancement factor does not have considerable effect.

5 Process analysis

This analysis is performed using the validated model. By changing a factor and fixing the other factors the respond of the model is examined.

5.1 Effect of rotor speed

Rotating speed impact on the absorption performance of an RPB absorber has been evaluated in existing studies. The results implies that it can improve heat and mass transfer performance in the RPB absorber. It is, therefore, important to understand how key process variables respond to the changes in rotating speed. Insights from this analysis can be used to predict the appropriate rotor speed for the RPB.

Hence, different case studies are considered to investigate the effect of rotor speed on CO_2 capture. For this purpose, this effect is analysed by considering two different concentrations of MEA in lean MEA solution (namely 55 and 75 wt.%.). The rotor speed changed from 400 to 1200 RPM by 200 step size and two lean MEA solution temperatures of 20 ^oC and 40 ^oC. For the lean MEA solution flow rate, the average flow rate of 30 L/min has been used. It must be mentioned that in process analysis, L/min has been used for flow rate because it make more sensible and realizable values.

The effect of rotor speed by changing from 400 to 1200 RPM is presented for two MEA concentrations in Figure 5. As it is obvious, in both concentrations by increasing the rotor speed the CO_2 capture level is increased. This is due to the improved mass transfer rate in the system by increasing the rotor speed. According to these figures, the liquid temperature has an effect on the CCL% at different rotor speed. In can be seen that in both cases namely 55 and 75 wt.% the increase of CCL% for 20 ^oC is more significant by increasing rotor speed in comparison with 40 ^oC. In case (a) at 20 ^oC the CCL% increase from 76.29% to 96.79% as rotor speed increases and in case (b) at 20 ^oC the CCL% increases from 83.18% to 98.51%.

The results showed that the CCL increases significantly between 400 to 800 RPM, but slows down as the rotor speed increases above 800 RPM. This can be seen for both MEA concentration in lean MEA solution and lean MEA solution temperatures. Rotational speed enhances mass transfer but at the same time increases the gas phase pressure drop (Jassim et al 2007). At rotor speed below 800 RPM, the results indicate that mass transfer enhancement is dominant but as rotor speed increases further the interfacial area decreases significantly and this slows down the mass transfer enhancement.

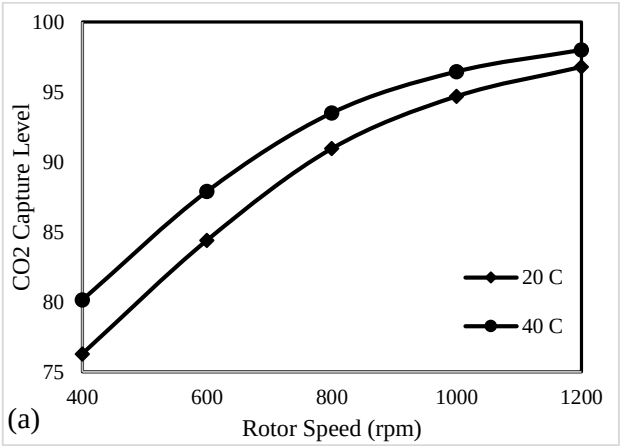

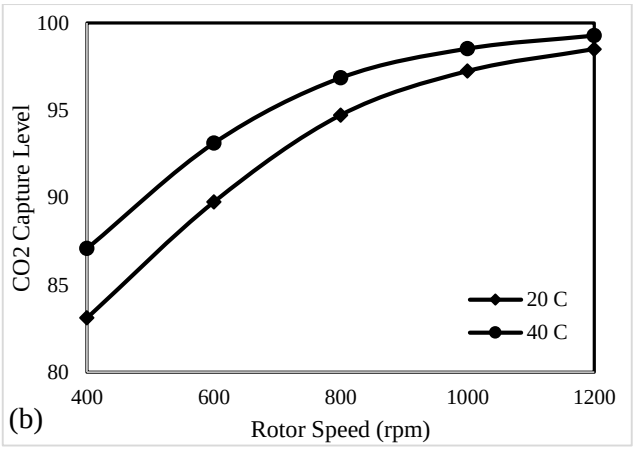

Figure 5: Effect of rotor speed on CCL% by using (a) 55 wt.% and (b) 75 wt.% lean MEA solutions.

5.2 Effect of MEA concentration in lean MEA solution

MEA concentration in lean MEA solution has an important effect on the CO_2-MEA reaction chemistry. However, the high viscosity of more concentrated MEA solution could potentially hinder mass transfer performance. By studying the effect of MEA concentration in lean MEA solution, how the overall performance of the RPB absorber is affected by the competing effects of more rapid reaction rate and slower mass transfer rate can be shown.

In order to evaluate the effect of MEA concentration in lean MEA solution on CO_2 capture level, different cases are considered. Rotor speed is fixed on 600 and 1000 RPM, gas and lean MEA solution flow rate to the RPB absorber 2.87 kmol/hr and 30 L/min, respectively, gas stream temperature 47 ^oC and two lean MEA solution temperature 20 and 40 ^oC. MEA weight percent is changed from 55 to 75 wt.% by step size of 5 wt.%.

The results of this analysis are presented in Figure 6. Figure 6 (a) shows the effect of MEA concentrations at 55 to 75 wt.% at 20 ^oC by using two rotor speed. By increasing the MEA concentration in lean MEA solution the CCL% is increasing slightly for 1000 RPM and more considerably for 600 RPM. The effect of concentration in the latter case is more important and in the first case the rotor speed has more effect on the CCL%.

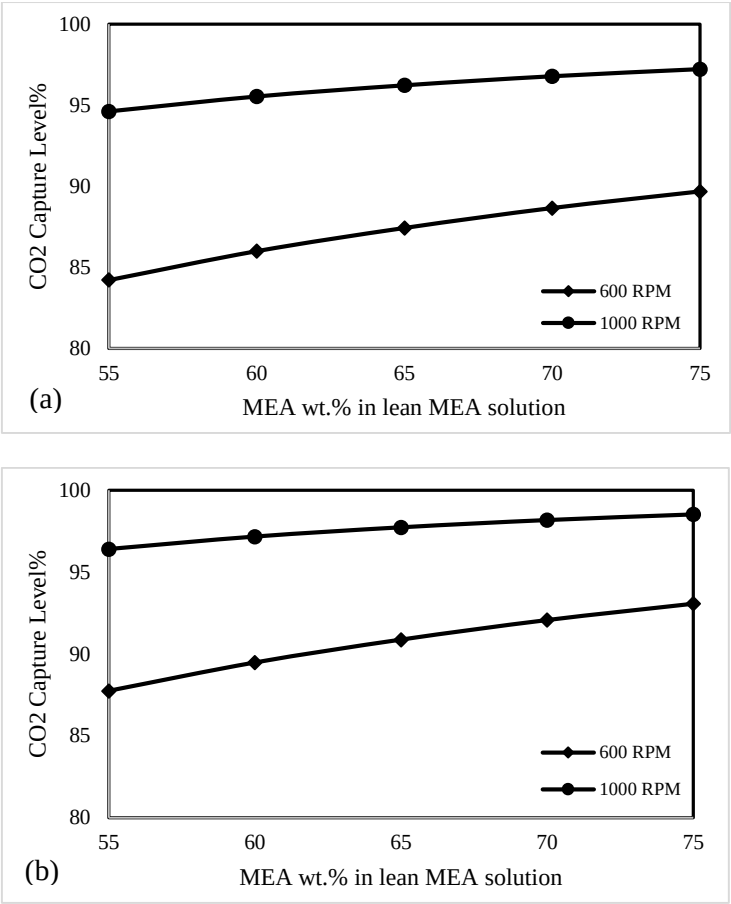

Figure 6: Effect of MEA wt.% in lean MEA solution on CCL% by using two different rotation speed (a) at 20 ^{o}C, (b) at 40 ^{o}C.

Figure 6 (b) shows the effect of MEA concentrations at 55 to 75 wt.% at 40 ^{o}C by using two rotor speed. As it can be seen the amount of CCL% in this case is higher than the CCL% presented in Figure 7 (a). Figure 6 (b) also shows the same trend; the increase of CCL% for 600 RPM is more significant than the increase of CCL% for 1000 RPM.

5.3 Effect of lean MEA solution temperature

The inlet lean MEA solution temperature could determine the extent of liquid phase temperature rise during absorption. The temperature rise increases the equilibrium partial pressure leading to the reduction of the CO_2 transfer from the gas phase to the liquid phase (Oko et al., 2018). In another aspect, higher lean MEA solution temperature could improve the reaction kinetics. Through this analysis, the overall impact on the RPB absorber performance can be demonstrated and appropriate operating lean MEA solution temperature can be predicted.

In order to examine the effect of lean MEA solution temperature, different cases are considered. The temperature changed from 20 to 60 ºC by a step size of 10 ºC. Two rotor speeds of 600 and 1000 RPM were considered. The average lean MEA solution flow rate of 30 l/min is used for the liquid phase. Two MEA concentrations of 55 and 75 wt.% are employed.

The effect of lean MEA solution temperature on CCL% is illustrated in Figure 7. Figure 7 (a), which is at 55 wt.% MEA, shows that temperature has more effect on CCL% at lower rotor speed. On the other hand, by increasing temperature of lean MEA solution the change in CCL% for 1000 RPM is not significant. The same results can be seen in Figure 7 (b). The chemical reaction rate is a function of lean MEA solution temperature, hence, increasing temperature of lean MEA solution improves the chemical reaction rate, and, consequently, enhances the CCL%.

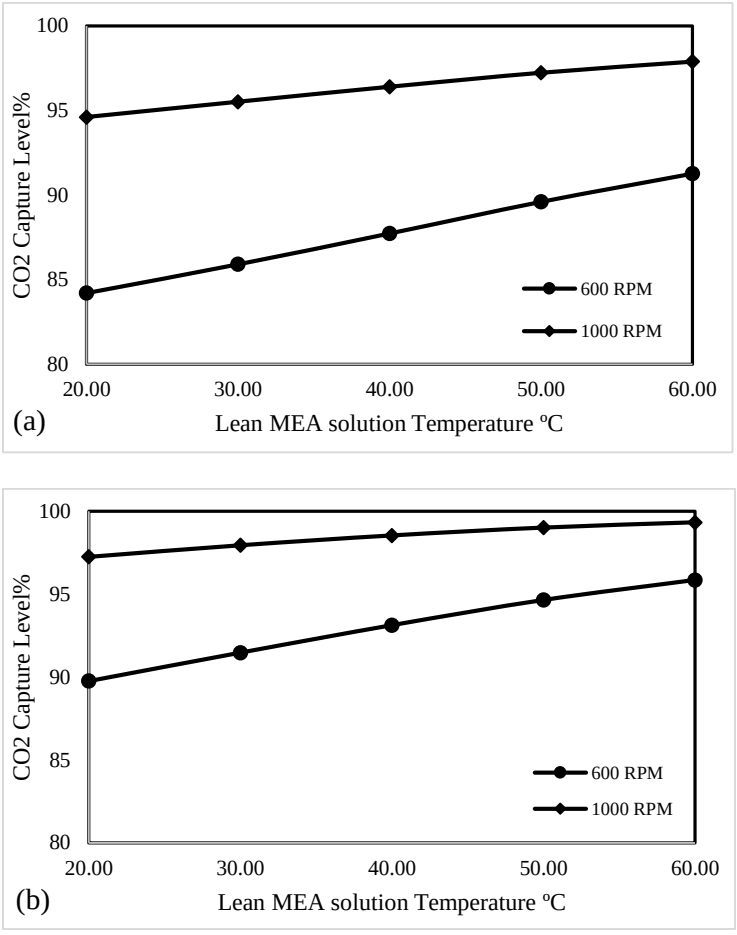

Figure 7: Effect of lean MEA solution temperature on CCL% by using two different rotation speed (a) at 55 wt.% MEA, (b) at 75 wt.% MEA.

5.4 Effect of lean MEA solution flow rate

The lean MEA flow rate often changes in accordance with the gas flowrate to maintain appropriate L/G ratio to avoid flooding and achieve desired capture level. This analysis will show how the system performance fluctuates in the event of changes in the lean MEA solution flow rate. Therefore, the lean MEA solution flow rate changed from 20 to 40 L/min by 5 L/min step size. The average lean MEA solution temperature of 30 ^{o}C, two rotor speeds of 600 and 1000 RPM, and also two MEA concentrations of 55 and 75 wt.% is applied.

Figure 8 (a) and (b) demonstrate the effect of changing liquid phase flow rate on CCL% at two different rotor speeds for 55 and 75 wt.%, respectively. Here, again, the change of CCL% by liquid flow rate for 600 RPM rotor speed is more significant in comparison with 1000 RPM. At 600 RPM increasing liquid flow rate enhances the mass transfer and also chemical reaction in the system. At 1000 RPM the effect of rotation on mass transfer is considerable which dominated the effect of the increase in liquid flow rate. The enhancement of CCL% is more significant for 600 RPM and 55 wt.% compared to the case of 600 RPM and 75 wt.%. In the first case, the CCL% changes from 80.75% to 88.92%, and in the second case, CCL% varies from 87.49% to 93.66%. This result is due to increased viscosity of liquid phase by rising MEA concentration, and, therefore, decreasing the mass transfer of CO_2 from the gas phase to liquid phase.

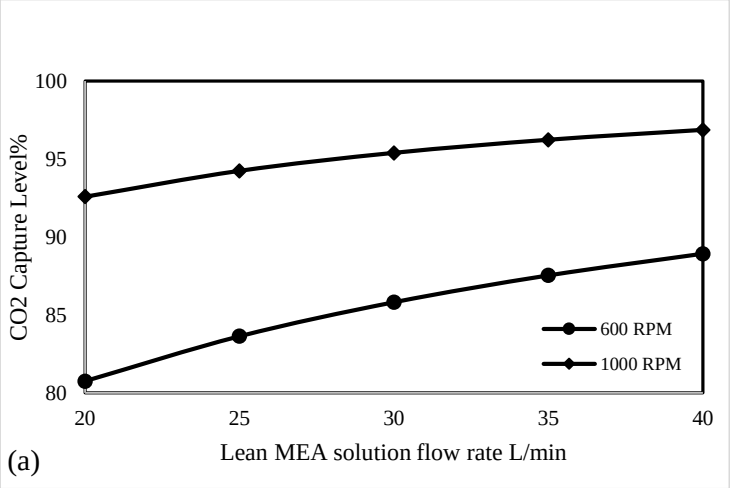

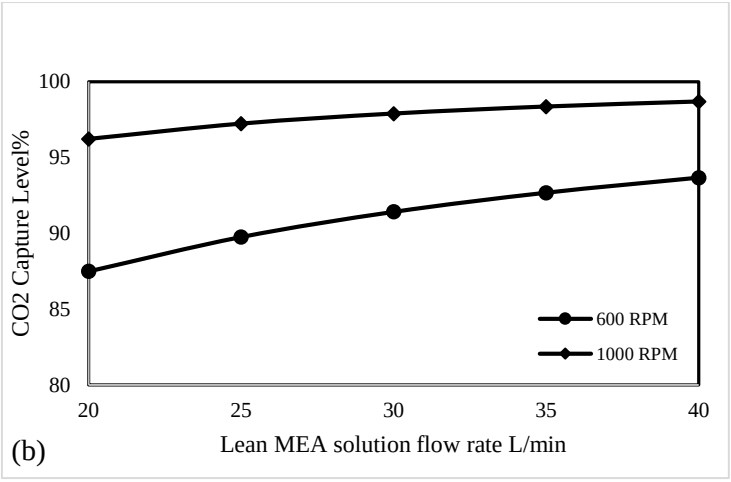

Figure 8: Effect of lean MEA solution flow rate on CCL% by using two different rotation speed (a) at 55 wt.% MEA, (b) at 75 wt.% MEA.

6 Multivariable sensitivity analysis

In this section, the simultaneous effect of four factors namely the MEA concentration in lean MEA solution, rotor speed, lean MEA solution temperature, and the lean MEA solution flow rate on CCL and motor power of the RPB absorber is examined using the orthogonal array design (OAD) (Taguchi et al., 1987). The OAD method is a statistical method that can be used to find the desirable operating condition of a system with respect to different input conditions (Afkhamipour and Mofarahi, 2018). Minitab® V17 has been used to carry out this study. The combination of four factors and five levels are presented in Table 10.

Table 10: The selected factors and their levels for CCL% and motor power.

Factors	Level 1	Level 2	Level 3	Level 4	Level 5
Rotor Speed (RPM)	400	600	800	1000	1200
MEA Concentration (wt.%)	55	60	65	70	75
Liquid temperature (°C)	20	30	40	50	60
Liquid flow rate (L/min)	20	25	30	35	40

According to Table 10, five levels are considered for four factors and inserted to the Minitab®. The OAD method is utilized to make a combination matrix for these levels and factors (the first fifth columns of Table 11) and make different scenarios. Each row of the first fifth columns of Table 11 are inserted to the model developed in gPROMS and value of CCL% and motor power are predicted. Therefore,

CCL% and motor power are regarded as the target output variable while MEA concentration in lean MEA solution, rotor speed, lean MEA solution temperature, and lean MEA solution flow rate are selected as the input conditions. The amount of power that consumed by motor of RPB absorber is estimated using a correlation proposed in literature (Singh et al., 1992):

$$P_{motor} = 1.2 + 0.1833 \times 10^{-7} \rho_l R_o^2 \omega^2 Q_l' \quad (24)$$

where P_{motor} is motor power (kW), ρ_l is density of liquid phase (kg/m^3), R_o is the outer radius of RPB (m), ω is angular velocity (rad/s), and Q_l' is volumetric flow rate of lean MEA solution (L/min).

Table 11: OAD and the results of CCL% and motor power from model developed in gPROMS.

	Inputs to the gPROMS model				Outputs of the gPROMS model		
Run	**Rotor Speed (rpm)**	**$C_{l,MEA}$ (wt.%)**	**T_l (°C)**	**Q_l' (L/min)**	**P_{motor} (kW)**	**CCL%**	**SNR**
1	400	55	20	20	145.595	65.94	36.38
2	400	60	30	25	180.391	73.77	37.36
3	400	65	40	30	214.668	80.68	38.14
4	400	70	50	35	247.891	86.67	38.76
5	400	75	60	40	280.154	91.39	39.22
6	600	60	20	30	486.449	85.88	38.68
7	600	65	30	35	563.418	90.47	39.13
8	600	70	40	40	637.896	94.09	39.47
9	600	75	50	20	318.285	91.46	39.22
10	600	55	60	25	401.214	89.40	39.03
11	800	65	20	40	1146.863	95.10	39.56
12	800	70	30	20	573.305	92.26	39.30
13	800	75	40	25	707.737	95.92	39.64
14	800	55	50	30	857.805	93.36	39.40
15	800	60	60	35	988.983	97.30	39.76
16	1000	70	20	25	1120.574	95.78	39.63
17	1000	75	30	30	1330.073	97.86	39.81
18	1000	55	40	35	1562.720	97.01	39.74
19	1000	60	50	40	1770.769	98.63	39.88
20	1000	65	60	20	885.988	97.63	39.79
21	1200	75	20	35	2240.795	98.84	39.90
22	1200	55	30	40	2580.760	98.32	39.85
23	1200	60	40	20	1291.131	97.08	39.74
24	1200	65	50	25	1596.318	98.85	39.90
25	1200	70	60	30	1894.319	99.59	39.96

By having CCL% values (obtained from process model in Section 2) for each row in the orthogonal matrix shown in Table 11 and the factors, the signal to noise ratio (SNR) values were calculated in Minitab® to analyse the results. The SNR is a measure of robustness used to identify control factors that reduce variability in a product or process by minimizing the effects of uncontrollable factors (noise

factors). Higher values of the signal to noise ratio (SNR) identify control factor settings that minimize the effects of the noise factors.

The importance of each factor on CCL% is determined based on ANOVA table (Table 12). P-values are the parameter to realize the importance of each factor. Smaller values of P-values show the greater importance of factor. F-values is a value to find out if the means between two populations are significantly different. All the factors are important, but rotor speed has the most important effect on the results, and after that liquid flow rate has the second importance.

Table 12: Analysis of variance for SNR of CCL% and motor power.

Factor	Degree of freedom	Sum of squares	Mean square	F-values	P-values
MEA Concentration (wt.%)	4	1.46	0.36	3.21	0.075
Rotor Speed (RPM)	4	11.97	2.99	26.28	0.001
Liquid temperature (^{o}C)	4	1.58	0.39	3.47	0.063
Liquid flow rate (L/min)	4	1.68	0.42	3.69	0.055
Residual Error	4	0.91	0.11	-	-
Total	24	17.60	-	-	-

In CO_2 capture studies, the 90% of CCL are considered as a proper value of capture level (Lawal et al., 2010). Therefore, according to Table 11, Runs number 5, 7, 9, 10, 12, and 14 which resulted in almost 90% CCL are selected to be compared in aspect of motor power. As can be seen, the less amount of motor power is consumed by case 5 but its CCL% is higher than cases 7 and 10 with motor power of 563.418 and 401.214 kW, respectively. It is interesting that case 7 consumes twice energy of case 5 but resulted in less value of CCL%. If the rotor speed increase almost three times (Run 10) in compare with Run 5, the value of CCL% increased only about 2%. As can be seen, the OAD method can provide different scenario and combination of factors affecting on CCL% and motor power and help to find the proper combination of four factors that resulted in the low motor power.

7 Conclusion

In this paper, a detailed first principle rate-based steady state model for RPB absorber is developed, and implemented in gPROMS® model builder. The effect of chemical reactions is accounted in the liquid phase by using kinetic rate reaction and enhancement factor. Different relations presented in the

literature to calculate the rate constant and enhancement factors are collected and examined. As correlations and physical properties have a significant impact on the model performance, properly validated models for high MEA concentration are selected. The process analysis performed based on changing rotor speed, MEA concentration in lean MEA solution, lean MEA solution temperature and lean MEA solution flow rates. The model results showed a very good agreement with the experimental data. ARD% between the experimental and the predicted CCL% value is changing between 0.79 and 6.97 and the AARD% for them is 3.50. In addition, the AD% between the experimental and the predicted fractions of CO_2 in the gas phase is changing between 0.03 and 0.26, and the AAD% for them is 0.14. The findings indicate that the kinetic model has significant effect on the model results but the enhancement factor relation is not much influential. All the process analysis results show a consistent trend. The OAD method results show that the rotor speed and lean MEA solution flow rate are the most dominant factors affecting the amount of CCL%. Furthermore, the proper combination of factors that resulted in almost 90% CCL and low motor power of RPB absorber can be achieved by using OAD method. Modelling of RPB system will be helpful in scale-up, optimization, troubleshooting, optimum design and process analysis of this system.

Acknowledgment

The authors acknowledge financial support from UK Engineering and Physical Sciences Research Council (EPSRC) (Ref: EP/M001458/2).

References

Aboudheir, A., Tontiwachwuthikul, P., Chakma, A., Idem, R., 2003. Kinetics of the reactive absorption of carbon dioxide in high CO2-loaded, concentrated aqueous monoethanolamine solutions. Chemical Engineering Science 58(23), 5195-5210.

Afkhamipour, M., Mofarahi, M., 2013. Comparison of rate-based and equilibrium-stage models of a packed column for post-combustion CO2 capture using 2-amino-2-methyl-1-propanol (AMP) solution. International Journal of Greenhouse Gas Control 15, 186-199.

Afkhamipour, M., Mofarahi, M., 2018. A modeling-optimization framework for assessment of CO2 absorption capacity by novel amine solutions: 1DMA2P, 1DEA2P, DEEA, and DEAB. Journal of Cleaner Production 171, 234-249.

Agbonghae, E.O., Hughes, K.J., Ingham, D.B., Ma, L., Pourkashanian, M., 2014. A Semi-Empirical Model for Estimating the Heat Capacity of Aqueous Solutions of Alkanolamines for CO2 Capture. Industrial & Engineering Chemistry Research 53(19), 8291-8301.

Arias, A.M., Mores, P.L., Scenna, N.J., Mussati, S.F., 2016. Optimal design and sensitivity analysis of post-combustion CO2 capture process by chemical absorption with amines. Journal of Cleaner Production 115, 315-331.

Barreau, A., Le Bouhelec, E.B., Tounsi, K.H., Mougin, P., Lecomte, F., 2006. Absorption of H2S and CO2 in alkanolamine aqueous solution: Experimental data and modelling with the electrolyte-NRTL model. Oil & Gas Science and Technology-Revue de l'IFP 61(3), 345-361.
Billet, R., Schultes, M., 1999. Prediction of Mass Transfer Columns with Dumped and Arranged Packings: Updated Summary of the Calculation Method of Billet and Schultes. Chemical Engineering Research and Design 77(6), 498-504.
Borhani, T.N.G., Afkhamipour, M., Azarpour, A., Akbari, V., Emadi, S.H., Manan, Z.A., 2016. Modeling study on CO2 and H2S simultaneous removal using MDEA solution. Journal of Industrial and Engineering Chemistry 34, 344-355.
Borhani, T.N.G., Azarpour, A., Akbari, V., Wan Alwi, S.R., Manan, Z.A., 2015. CO2 capture with potassium carbonate solutions: A state-of-the-art review. International Journal of Greenhouse Gas Control 41(Supplement C), 142-162.
Burns, J.R., Jamil, J.N., Ramshaw, C., 2000. Process intensification: operating characteristics of rotating packed beds — determination of liquid hold-up for a high-voidage structured packing. Chemical Engineering Science 55(13), 2401-2415.
Caplow, M., 1968. Kinetics of carbamate formation and breakdown. Journal of the American Chemical Society 90(24), 6795-6803.
Cheng, H.-H., Lai, C.-C., Tan, C.-S., 2013. Thermal regeneration of alkanolamine solutions in a rotating packed bed. International Journal of Greenhouse Gas Control 16, 206-216.
Chilton, T.H., Colburn, A.P., 1934. Mass transfer (absorption) coefficients prediction from data on heat transfer and fluid friction. Industrial & engineering chemistry 26(11), 1183-1187.
Crooks, J.E., Donnellan, J.P., 1989. Kinetics and mechanism of the reaction between carbon dioxide and amines in aqueous solution. Journal of the Chemical Society, Perkin Transactions 2(4), 331-333.
da Silva, E.F., Svendsen, H.F., 2004. Ab Initio Study of the Reaction of Carbamate Formation from CO2 and Alkanolamines. Industrial & Engineering Chemistry Research 43(13), 3413-3418.
Danckwerts, P.V., 1970. Gas-liquid reactions. McGraw-Hill, New York.
Danckwerts, P.V., 1979. The reaction of CO2 with ethanolamines. Chemical Engineering Science 34(4), 443-446.
Ebadi Amooghin, A., Mehdi, M.S.M., Mona, Z.P., 2017. Rigorous modeling of gas permeation behavior in facilitated transport membranes (FTMs); evaluation of carrier saturation effects and double-reaction mechanism. Greenhouse Gases: Science and Technology 0(0).
Fairbanks, D.F., Wilke, C.R., 1950. Diffusion Coefficients in Multicomponent Gas Mixtures. Industrial & Engineering Chemistry 42(3), 471-475.
Faramarzi, L., Kontogeorgis, G.M., Michelsen, M.L., Thomsen, K., Stenby, E.H., 2010. Absorber Model for CO2 Capture by Monoethanolamine. Industrial & Engineering Chemistry Research 49(8), 3751-3759.
Fuller, E.N., Schettler, P.D., Giddings, J.C., 1966. NEW METHOD FOR PREDICTION OF BINARY GAS-PHASE DIFFUSION COEFFICIENTS. Industrial & Engineering Chemistry 58(5), 18-27.
Gabrielsen, J., Michelsen, M.L., Stenby, E.H., Kontogeorgis, G.M., 2005. A Model for Estimating CO2 Solubility in Aqueous Alkanolamines. Industrial & Engineering Chemistry Research 44(9), 3348-3354.
Hanley, B., Chen, C.-C., 2012. New mass-transfer correlations for packed towers. AIChE Journal 58(1), 132-152.
Harker, J.H., Backhurst, J.R., Richardson, J.F., 2003. Chemical Engineering. Elsevier Science.
Harun, N., 2012. Dynamic Simulation of MEA Absorption Process for CO2 Capture from Power Plants. UWSpace.
Harun, N., Nittaya, T., Douglas, P.L., Croiset, E., Ricardez-Sandoval, L.A., 2012. Dynamic simulation of MEA absorption process for CO2 capture from power plants. International Journal of Greenhouse Gas Control 10(Supplement C), 295-309.
Hikita, H., Asai, S., Ishikawa, H., Honda, M., 1977. The kinetics of reactions of carbon dioxide with monoethanolamine, diethanolamine and triethanolamine by a rapid mixing method. The Chemical Engineering Journal 13(1), 7-12.
Horng, S.-Y., Li, M.-H., 2002. Kinetics of Absorption of Carbon Dioxide into Aqueous Solutions of Monoethanolamine + Triethanolamine. Industrial & Engineering Chemistry Research 41(2), 257-266.
Hsu, C.-H., Li, M.-H., 1997. Densities of Aqueous Blended Amines. Journal of Chemical & Engineering Data 42(3), 502-507.

Jassim, M.S., 2002. Process intensification: Absorption and desorption of carbon dioxide from monoethanolamine solutions using HiGee technology. Newcastle University.
Jassim, M.S., Rochelle, G., Eimer, D., Ramshaw, C., 2007. Carbon Dioxide Absorption and Desorption in Aqueous Monoethanolamine Solutions in a Rotating Packed Bed. Industrial & Engineering Chemistry Research 46(9), 2823-2833.
Joel, A.S., Wang, M., Ramshaw, C., 2015. Modelling and simulation of intensified absorber for post-combustion CO2 capture using different mass transfer correlations. Applied Thermal Engineering 74, 47-53.
Joel, A.S., Wang, M., Ramshaw, C., Oko, E., 2014. Process analysis of intensified absorber for post-combustion CO2 capture through modelling and simulation. International Journal of Greenhouse Gas Control 21, 91-100.
Joel, A.S., Wang, M., Ramshaw, C., Oko, E., 2017. Modelling, simulation and analysis of intensified regenerator for solvent based carbon capture using rotating packed bed technology. Applied Energy 203, 11-25.
Kale, C., Górak, A., Schoenmakers, H., 2013. Modelling of the reactive absorption of CO2 using mono-ethanolamine. International Journal of Greenhouse Gas Control 17(0), 294-308.
Kang, J.-L., Sun, K., Wong, D.S.-H., Jang, S.-S., Tan, C.-S., 2014. Modeling studies on absorption of CO2 by monoethanolamine in rotating packed bed. International Journal of Greenhouse Gas Control 25, 141-150.
Kang, J.-L., Wong, D.S.-H., Jang, S.-S., Tan, C.-S., 2016. A comparison between packed beds and rotating packed beds for CO2 capture using monoethanolamine and dilute aqueous ammonia solutions. International Journal of Greenhouse Gas Control 46, 228-239.
Kvamsdal, H.M., Jakobsen, J.P., Hoff, K.A., 2009. Dynamic modeling and simulation of a CO2 absorber column for post-combustion CO2 capture. Chemical Engineering and Processing: Process Intensification 48(1), 135-144.
Lawal, A., Wang, M., Stephenson, P., Koumpouras, G., Yeung, H., 2010. Dynamic modelling and analysis of post-combustion CO2 chemical absorption process for coal-fired power plants. Fuel 89(10), 2791-2801.
Liu, Y., Fan, W., Wang, K., Wang, J., 2016. Studies of CO2 absorption/regeneration performances of novel aqueous monothanlamine (MEA)-based solutions. Journal of Cleaner Production 112, 4012-4021.
Llano-Restrepo, M., Araujo-Lopez, E., 2015. Modeling and simulation of packed-bed absorbers for post-combustion capture of carbon dioxide by reactive absorption in aqueous monoethanolamine solutions. International Journal of Greenhouse Gas Control 42(Supplement C), 258-287.
Llerena-Chavez, H., Larachi, F., 2009. Analysis of flow in rotating packed beds via CFD simulations—Dry pressure drop and gas flow maldistribution. Chemical Engineering Science 64(9), 2113-2126.
Luo, X., Hartono, A., Hussain, S., F. Svendsen, H., 2015. Mass transfer and kinetics of carbon dioxide absorption into loaded aqueous monoethanolamine solutions. Chemical Engineering Science 123(Supplement C), 57-69.
Luo, X., Hartono, A., Svendsen, H.F., 2012. Comparative kinetics of carbon dioxide absorption in unloaded aqueous monoethanolamine solutions using wetted wall and string of discs columns. Chemical Engineering Science 82(Supplement C), 31-43.
Moftakhari Sharifzadeh, M.M., Ebadi Amooghin, A., Zamani Pedram, M., Omidkhah, M., 2016. Time-dependent mathematical modeling of binary gas mixture in facilitated transport membranes (FTMs): A real condition for single-reaction mechanism. Journal of Industrial and Engineering Chemistry 39, 48-65.
Oko, E., Ramshaw, C., Wang, M., 2018. Study of intercooling for rotating packed bed absorbers in intensified solvent-based CO2 capture process. Applied Energy 223, 302-316.
Onda, K., Takeuchi, H., Okumoto, Y., 1968. Mass transfer coefficients between gas and liquid phases in packed columns. Journal of Chemical Engineering of Japan 1(1), 56-62.
Porter, K., 1966. EFFECT OF CONTACT-TIME DISTRIBUTION ON GAS ABSORPTION WITH CHEMICAL REACTION. TRANSACTIONS OF THE INSTITUTION OF CHEMICAL ENGINEERS AND THE CHEMICAL ENGINEER 44(1), T25-&.
Prausnitz, J.M., Lichtenthaler, R.N., de Azevedo, E.G., 1998. Molecular Thermodynamics of Fluid-Phase Equilibria. Pearson Education.

Putta, K.R., Tobiesen, F.A., Svendsen, H.F., Knuutila, H.K., 2017. Applicability of enhancement factor models for CO2 absorption into aqueous MEA solutions. Applied Energy 206, 765-783.
Qian, Z., Xu, L.-B., Li, Z.-H., Li, H., Guo, K., 2010. Selective Absorption of H2S from a Gas Mixture with CO2 by Aqueous N-Methyldiethanolamine in a Rotating Packed Bed. Industrial & Engineering Chemistry Research 49(13), 6196-6203.
Qian, Z., Xu, L., Cao, H., Guo, K., 2009. Modeling Study on Absorption of CO2 by Aqueous Solutions of N-Methyldiethanolamine in Rotating Packed Bed. Industrial & Engineering Chemistry Research 48(20), 9261-9267.
Singh, S.P., Wilson, J.H., Counce, R.M., Lucero, A.J., Reed, G.D., Ashworth, R.A., Elliott, M.G., 1992. Removal of volatile organic compounds from groundwater using a rotary air stripper. Industrial & engineering chemistry research 31(2), 574-580.
Snijder, E.D., te Riele, M.J.M., Versteeg, G.F., van Swaaij, W.P.M., 1993. Diffusion coefficients of several aqueous alkanolamine solutions. Journal of Chemical & Engineering Data 38(3), 475-480.
Taguchi, G., Konishi, S., Konishi, S., Institute, A.S., 1987. Orthogonal Arrays and Linear Graphs: Tools for Quality Engineering. American Supplier Institute.
Tsai, T.-C., Ko, J.-J., Wang, H.-M., Lin, C.-Y., Li, M.-H., 2000. Solubility of Nitrous Oxide in Alkanolamine Aqueous Solutions. Journal of Chemical & Engineering Data 45(2), 341-347.
Tung, H.-H., Mah, R.S.H., 1985. MODELING LIQUID MASS TRANSFER IN HIGEE SEPARATION PROCESS. Chemical Engineering Communications 39(1-6), 147-153.
Vaidya, P.D., Kenig, E.Y., 2007. CO2-Alkanolamine Reaction Kinetics: A Review of Recent Studies. Chemical Engineering & Technology 30(11), 1467-1474.
van Krevelen, D.W., Hoftijzer, P.J., 1948. Kinetics of gas-liquid reactions part I. General theory. Recueil des Travaux Chimiques des Pays-Bas 67(7), 563-586.
van Swaaij, W.P.M., Versteeg, G.F., 1992. Mass transfer accompained with complex reversible chemical reactions in gas-liquid systems: An overview. Chemical Engineering Science 47(13-14), 3181-3195.
Versteeg, G.F., Van Dijck, L.A.J., Van Swaaij, W.P.M., 1996. ON THE KINETICS BETWEEN CO2 AND ALKANOLAMINES BOTH IN AQUEOUS AND NON-AQUEOUS SOLUTIONS. AN OVERVIEW. Chemical Engineering Communications 144(1), 113-158.
Versteeg, G.F., Van Swaaij, W.P.M., 1988. Solubility and diffusivity of acid gases (carbon dioxide, nitrous oxide) in aqueous alkanolamine solutions. Journal of Chemical & Engineering Data 33(1), 29-34.
Wang, M., Joel, A.S., Ramshaw, C., Eimer, D., Musa, N.M., 2015. Process intensification for post-combustion CO2 capture with chemical absorption: A critical review. Applied Energy 158, 275-291.
Wang, Y.W., Xu, S., Otto, F.D., Mather, A.E., 1992. Solubility of N2O in alkanolamines and in mixed solvents. The Chemical Engineering Journal 48(1), 31-40.
Weiland, R.H., Dingman, J.C., Cronin, D.B., Browning, G.J., 1998. Density and Viscosity of Some Partially Carbonated Aqueous Alkanolamine Solutions and Their Blends. Journal of Chemical & Engineering Data 43(3), 378-382.
Weiland, R.H., Rawal, M., Rice, R.G., 1982. Stripping of carbon dioxide from monoethanolamine solutions in a packed column. AIChE Journal 28(6), 963-973.
Wellek, R.M., Brunson, R.J., Law, F.H., 1978. Enhancement factors for gas-absorption with second-order irreversible chemical reaction. The Canadian Journal of Chemical Engineering 56(2), 181-186.
Wilke, C.R., Chang, P., 1955. Correlation of diffusion coefficients in dilute solutions. AIChE Journal 1(2), 264-270.
Yeramian, A.A., Gottifredi, J.C., Ronco, J.J., 1970. Mass transfer with homogeneous second order irreversible reaction a note on an explicit expression for the reaction factor. Chemical Engineering Science 25(10), 1622-1625.
Yi, F., Zou, H.-K., Chu, G.-W., Shao, L., Chen, J.-F., 2009. Modeling and experimental studies on absorption of CO2 by Benfield solution in rotating packed bed. Chemical Engineering Journal 145(3), 377-384.
Ying, J., Eimer, D.A., 2012. Measurements and Correlations of Diffusivities of Nitrous Oxide and Carbon Dioxide in Monoethanolamine + Water by Laminar Liquid Jet. Industrial & Engineering Chemistry Research 51(50), 16517-16524.

Ying, J., Eimer, D.A., 2013. Determination and Measurements of Mass Transfer Kinetics of CO2 in Concentrated Aqueous Monoethanolamine Solutions by a Stirred Cell. Industrial & Engineering Chemistry Research 52(7), 2548-2559.
Ying, J., Eimer, D.A., Wenjuan, Y., 2012. Measurements and Correlation of Physical Solubility of Carbon Dioxide in (Monoethanolamine + Water) by a Modified Technique. Industrial & Engineering Chemistry Research 51(19), 6958-6966.
Yu, C.-H., Cheng, H.-H., Tan, C.-S., 2012. CO2 capture by alkanolamine solutions containing diethylenetriamine and piperazine in a rotating packed bed. International Journal of Greenhouse Gas Control 9, 136-147.